

1 A manuscript uploaded to BG as a production file (bg-2016-222)

2

3

4 Manganese and iron reduction dominate organic carbon oxidation in surface
5 sediments of the deep Ulleung Basin, East Sea

6

7

8 Jung-Ho Hyun^{1*}, Sung-Han Kim¹, Jin-Sook Mok¹, Hyeyoun Cho¹, Tongsup Lee², Verona
9 Vandieken³ and Bo Thamdrup^{4*}

10

11

12 ¹Department of Marine Science and Convergence Engineering, Hanyang University, 55
13 Hanyangdaehak-ro, Ansan, Gyeonggi-do 15588, South Korea

14

15 ²Department of Oceanography, Pusan National University, 2 Busandaehak-ro, Busan, 46241,
16 South Korea

17

18 ³Institute for Chemistry and Biology of the Marine Environment, University of Oldenburg,
19 Carl-von-Ossietzky-Str. 9-11, 26129 Oldenburg, Germany

20

21 ⁴Nordic Center for Earth Evolution, Department of Biology, University of Southern Denmark,
22 Campusvej 55, 5230 Odense M, Denmark

23

24

25 *Correspondence to:

26 Jung-Ho Hyun (hyunjh@hanyang.ac.kr)

27 Bo Thamdrup (bot@biology.sdu.dk)

28

29

30

31 **Abstract.** Rates and pathways of benthic organic carbon (C_{org}) oxidation were investigated in
32 surface sediments of the Ulleung Basin (UB) characterized by high C_{org} contents ($> 2.5 \%$,
33 dry wt.) and very high contents of Mn oxides ($> 200 \mu\text{mol cm}^{-3}$) and Fe oxides (up to 100
34 $\mu\text{mol cm}^{-3}$). The combination of geochemical analyses and independently executed metabolic
35 rate measurements revealed that Mn and Fe reduction were the dominant C_{org} oxidation
36 pathways in the center of the UB, comprising 45% and 20% of total C_{org} oxidation,
37 respectively. By contrast, sulfate reduction was the dominant C_{org} oxidation pathway
38 accounting for 50% of total C_{org} mineralization in sediments of the continental slope. The
39 relative significance of each C_{org} oxidation pathway matched the depth distribution of the
40 respective electron acceptors. The relative importance of Mn reduction for C_{org} oxidation
41 displays saturation kinetics with respect to Mn oxide content with a low half-saturation value
42 of $8.6 \mu\text{mol cm}^{-3}$, which further implies that Mn reduction can be a dominant C_{org} oxidation
43 process even in sediments with lower MnO_2 content as known from several other locations.
44 This is the first report of a high contribution of manganese reduction to C_{org} oxidation in
45 offshore sediments on the Asian margin. The high manganese oxide content in the surface
46 sediment in the central UB was maintained by an extreme degree of recycling, with each Mn
47 atom on average being reoxidized ~ 3800 times before permanent burial. This is the highest
48 degree of recycling so far reported for Mn-rich sediments, and it appears linked to the high
49 benthic mineralization rates resulting from the high C_{org} content that indicate the UB as a
50 biogeochemical hotspot for turnover of organic matter and nutrient regeneration.

51

52

53 **Keywords.** Benthic mineralization, Manganese reduction, Iron reduction, Sulfate reduction,
54 Ulleung Basin, East Sea

55

56 **1 Introduction**

57

58 Although they cover only 15 % (47×10^6 km²) of the ocean surface area, sediments of
59 continental margins (200–2000 m depth) are characterized by enhanced organic matter flux
60 generated either by vertical transport from the highly productive overlying water column or
61 by lateral transport from adjacent shelves, and thus play an important role in deposition and
62 mineralization of organic matter (Romankevich, 1984; Jahnke et al., 1990; Walsh, 1991;
63 Jahnke and Jahnke, 2000). Organic particles that reach the seafloor are quickly mineralized
64 by hydrolysis, fermentation, and a variety of respiratory processes using different electron
65 acceptors such as oxygen, nitrate, Mn oxides, Fe oxides, and sulfate (Froelich et al., 1979;
66 Jørgensen, 2006). The partitioning of organic carbon (C_{org}) oxidation among the different
67 electron accepting pathways has profound influence on the distribution and the release and/or
68 retention of Mn, Fe, S and nutrients (nitrogen and phosphate) (Canfield et al., 2005; Hansen
69 et al., 2006; Jørgensen, 2006; Slomp et al., 2013). Therefore, it is particularly important to
70 elucidate the contribution of each C_{org} oxidation pathway in order to better understand the
71 role of sediments in biogeochemical element cycles.

72 The relative significance of each carbon oxidation pathway is largely controlled by the
73 combination of organic matter supply and availability of electron acceptors. In general,
74 aerobic metabolism dominates the organic matter mineralization in deep-sea sediments that
75 are characterized by low organic matter content (Jahnke et al., 1982; Glud, 2008), especially
76 in organic carbon-starved deep-sea sediments with low sedimentation rates (Mewes et al.,
77 2014, 2016; D'Hondt et al. 2015; Mogollón et al., 2016). In contrast, owing to high sulfate
78 concentrations in marine sediment, sulfate reduction might account for up to 50 % of total
79 carbon oxidation in continental margins with high organic matter flux (Jørgensen, 1982;
80 Jørgensen and Kasten, 2006; Bowles et al., 2014). However, in sediments where manganese
81 and iron oxides are abundant or rapidly recycled, microbial reduction of manganese and iron
82 can be the dominant electron accepting processes over sulfate reduction (Sørensen and
83 Jørgensen, 1987; Aller, 1990; Canfield et al., 1993b). The significance of dissimilatory iron
84 reduction for C_{org} oxidation is well established in the sediments of various continental
85 margins and coastal wetlands (Thamdrup, 2000; Thamdrup and Canfield, 1996; Jensen et al.,
86 2003, Kostka et al., 2002a, 2002b; Vandieken et al., 2006; Hyun et al., 2007, 2009b).
87 However, only a few locations such as the Panama Basin (Aller, 1990), the coastal
88 Norwegian trough in Skagerrak and an adjacent fjord (Canfield et al., 1993a, 1993b;

89 Vandieken et al., 2014), the Black Sea shelf (Thamdrup et al., 2000) and the continental shelf
90 of the northern Barents Sea (Vandieken et al., 2006; Nickel et al., 2008) are known where
91 microbial manganese reduction significantly contributes to carbon mineralization.

92 The East Sea (often referred to as Japan Sea), located in the far eastern part of the Eurasian
93 continental margin, consists of three major basins deeper than 2000 m, the Japan Basin, the
94 Yamato Basin and the Ulleung Basin (Fig. 1). Compared to the other two basins, the surface
95 waters of the Ulleung Basin (UB) are characterized by higher phytoplankton biomass and
96 primary production (Yamada et al., 2005; Yoo and Park, 2009), which is associated with
97 coastal upwelling (Hyun et al., 2009a). The enhanced biological production in the euphotic
98 zone of the UB is responsible for the high C_{org} content (> 2.5 % wt) in the sediment, and the
99 highest rates of C_{org} oxidation compared to other deep-sea sediments with similar depth range
100 (Lee et al., 2008; Hyun et al., 2010). An intriguing geochemical property of the UB surface
101 sediment is the high content of Mn oxides ($> 200 \mu\text{mol cm}^{-3}$) and Fe oxides (up to $100 \mu\text{mol}$
102 cm^{-3}) (Cha et al., 2007; Hyun et al., 2010). In accordance with these geochemical findings,
103 the suppression of sulfate reduction (Hyun et al., 2010) and accumulation of Mn^{2+} in anoxic
104 incubation of surface sediment (Vandieken et al., 2012) strongly implied that the C_{org}
105 oxidation in the surface sediment of the UB is dominated by microbial manganese and iron
106 reduction, but actual rates and partitioning of each electron accepting pathway in C_{org}
107 oxidation remain to be determined in this deep marginal sediment underlying highly
108 productive surface waters.

109 The primary objective of this paper was to characterize the sediment biogeochemistry with
110 regard to the rate of C_{org} oxidation and partitioning of major terminal electron accepting
111 pathways at two contrasting sites at the continental slope and rise in the UB. Here, for the
112 first time in sediments of the Asian marginal seas, we document that Mn and Fe reduction are
113 the dominant C_{org} oxidation pathways accounting for respectively 45 % and 20 % of total C_{org}
114 oxidation in the center of the UB, and suggest that Mn and Fe reduction may be of greater
115 importance in deep-sea sediments than previously recognized.

116

117 **2 Materials and methods**

118

119 **2.1 Study site**

120

121 The East Sea is a marginal sea surrounded by the east Asian continent and Japanese Islands

122 (Fig. 1, Kang et al., 2010; Liu et al., 2010). The UB located in the southwestern part of the
123 East Sea is a bowl-shaped deep basin (2000–3000 m depth) (Fig. 1) delimited by continental
124 slopes of Korean Peninsula and the southwestern Japanese Archipelago on the west and south,
125 respectively, and by the Korea Plateau and the Oki Bank on the north and east, respectively
126 (Chough et al., 2000).

127 Shipboard experiments were conducted in June, 2009 at two sites on the continental slope
128 (Station M1, hereafter M1) and in the center (Station D3, hereafter D3) of the UB (Fig. 1,
129 Table 1). Surface sediments consist of fine-grained clay with a mean grain size less than
130 0.004 mm in diameter (Cha et al., 2007). Two stations were characterized by two contrasting
131 sediment colors. The Mn oxide-enriched surface sediment at the basin site (D3) was reddish-
132 brown, whereas at the slope site (M1) it exhibited the typical gray-brown color of muddy
133 continental margin sediments (Fig. 1). Further environmental properties are listed in Table 1.

134

135 **2.2 Sampling and handling**

136

137 Sediment samples were collected with a box corer. Onboard, duplicate or mostly triplicate
138 sub-samples for geochemical analyses were collected using acrylic cores (6–9 cm in diameter
139 and 30–40 cm in length). The sub-cores for geochemical analyses were immediately sealed
140 with butyl rubber stoppers and transferred to a N₂-filled glove bag for sectioning and loading
141 into polypropylene centrifuge tubes that were then tightly capped and centrifuged for 15 min
142 at 5000 × g. After reintroduction into the N₂-filled glove bag, pore-waters were sampled and
143 filtered through 0.2-μm cellulose ester syringe filters (ADVANTEC, Toyo Rashi Kaisha, Ltd).
144 One to two mL of pore water to determine NH₄⁺ was fixed with saturated HgCl₂, and frozen.
145 For determination of Fe²⁺, Mn, SO₄²⁻ and Ca²⁺, 2 mL of the pore water were acidified with 12
146 M HCl and stored at 4 °C. Pore-water for sulfide analysis was preserved with Zn acetate
147 (20 %). Sediments for solid-phase analysis were frozen at –25 °C for future analyses.

148

149 **2.3 Anoxic bag incubations**

150

151 Anaerobic carbon mineralization rates and dissimilatory Mn and Fe reduction rates were
152 determined in batch incubations based on the procedures of Canfield et al. (1993b) and
153 Thamdrup and Canfield (1996). Sediment cores were transferred to a N₂-filled glove bag and
154 sliced in 2-cm intervals to a depth of 10 cm. Sediment from parallel sections was pooled,

155 mixed and loaded into gas-tight plastic bags (Hansen et al., 2000). The bags were sealed
156 without gas space, and incubated in the dark at near in situ temperature (ca. 1–2 °C) in larger
157 N₂ filled bags to ensure anoxic conditions. Over a period of 18 days of incubation, sub-
158 samples to determine the accumulation of total dissolved inorganic carbon (DIC) and Mn in
159 pore water were withdrawn on days 0, 1, 3, 5, 9 and 18. Two 50-mL centrifuge tubes per bag
160 were filled completely with sediment in a N₂-filled glove bag, and pore-water was extracted
161 as described above. For DIC analysis, we collected 1.8 mL aliquots into glass vials without
162 head space, fixed with 18 µL of HgCl₂ (125 mM), and stored at 4 °C until analysis within 4
163 weeks. Samples for Mn analysis were acidified with 12 M HCl and stored at 4 °C. Sediment
164 remaining after the collection of pore water was frozen at –25 °C for later analysis of oxalate
165 extractable solid Fe(II).

166

167 **2.4 Pore-water analyses**

168

169 Total dissolved inorganic carbon (DIC) and NH₄⁺ were measured by flow injection analysis
170 with conductivity detection (Hall and Aller, 1992). Nitrate was measured
171 spectrophotometrically (Parsons et al., 1984). Dissolved Fe²⁺ was determined by colorimetric
172 method with Ferrozine (Stookey, 1970). Dissolved Mn²⁺ and Ca²⁺ were analyzed in acidified
173 pore water by inductively coupled plasma-atomic emission spectrometry (ICP-AES, Optima
174 3300DV, Perkin-Elmer Co.) and flame atomic absorption spectrometer (SpectrAA 220/FS,
175 Varian), respectively (Thamdrup and Canfield, 1996). Dissolved sulfide was determined by
176 the methylene blue method (Cline, 1969). Sulfate concentrations were measured using ion
177 chromatography (Metrohm 761). The detection limit of H₂S, Ca²⁺, Mn²⁺ and Fe²⁺ was 3 µM,
178 1.8 µM, 3 µM and 1 µM, respectively. Reproducibility of DIC and NH₄⁺ was better than
179 10 %. Precision of NO₃⁻ was 1–2 %.

180

181 **2.5 Solid-phase analyses**

182

183 Total oxalate-extractable Fe [Fe(II) + Fe(III)] was extracted from air-dried sediment in a 0.2
184 M oxalic acid solution (pH 3) for 4 h (Thamdrup and Canfield, 1996), and Fe(II) was
185 extracted from frozen sediment in anoxic oxalate (Phillips and Lovley, 1987). The total
186 oxalate-extractable Fe and Fe(II), hereafter total Fe_(oxal) and Fe(II)_(oxal), were determined as
187 described for the pore-water analysis of Fe²⁺. Oxalate-extractable Fe(III), hereafter

188 Fe(III)_(oxal), was defined as the difference between total Fe_(oxal) and Fe(II)_(oxal). This fraction
189 represents poorly crystalline Fe(III) oxides. Particulate Mn, hereafter Mn_(DCA) was extracted
190 with dithionite-citrate-acetic acid (DCA; pH 4.8) for 4 h from air-dried sediment and was
191 determined by inductively coupled plasma-atomic emission spectrometry (ICP-AES, Optima
192 3300DV, Perkin-Elmer Co). The DCA extraction aims at dissolving free Mn oxides and
193 authigenic Mn(II) phases. The reproducibility of the measurements was better than 10 % and
194 the detection limits was 3 μM for Mn and 1 μM for Fe. For the determination of total reduced
195 sulfur (TRS) that includes acid volatile sulfide (AVS = FeS + H₂S and small amounts of other
196 metal sulfides, see Rickard and Morse, 2005; Luther, 2005) and chromium-reducible sulfur
197 (CRS = S⁰ + FeS₂), sediment samples were fixed with Zn acetate, and sulfide was determined
198 according to the method of Cline (1969) after a two-step distillation with cold 12 M HCl and
199 boiling 0.5 M Cr²⁺ solution (Fossing and Jørgensen, 1989). The contents of total organic
200 carbon (TOC) and nitrogen (TN) in the surface sediment were analyzed using a CHN
201 analyzer (CE Instrument, EA 1110) after removing CaCO₃ using 12 M HCl.

202

203 **2.6 Oxygen micro-profiles**

204

205 Oxygen profiles were measured at 50 μm resolution using Clark-type microelectrodes
206 (Unisense, OX-50) while stirring the overlying water. Microelectrodes were calibrated
207 between 100 % air-saturated *in situ* bottom water and N₂ purged anoxic bottom water. Three
208 profiles were measured at each site. The diffusive boundary layer (DBL) and sediment-water
209 interface (SWI) were determined according to Jørgensen and Revsbech (1985). To estimate
210 the volume-specific oxygen consumption rate, we used the PROFILE software (Berg et al.,
211 1998).

212

213 **2.7 Rate measurements**

214

215 The diffusive oxygen uptake (DOU) was calculated from the calibrated oxygen microprofiles.

216

$$217 \text{DOU} = -D_o \times (\Delta C / \Delta z) \quad (1)$$

218

219 where D_o ($1.07 \times 10^{-9} \text{ m}^2 \text{ s}^{-1}$ at M1 and $1.03 \times 10^{-9} \text{ m}^2 \text{ s}^{-1}$ at D3) is the temperature-corrected
220 molecular diffusion coefficient estimated from Schulz (2006), and C is the oxygen

221 concentration at depth z within the diffusive boundary layer (DBL) (Jørgensen and Revsbech,
222 1985).

223 The volume-specific O_2 consumption rates exhibited a bimodal depth distribution (see
224 results section 3.2) with activity peaks near the SWI and the oxic/anoxic interface,
225 respectively. Thus, O_2 consumption rates by aerobic organotrophic respiration was defined as
226 the O_2 consumption rate near the SWI, whereas the oxygen consumption at the oxic-anoxic
227 interface was assigned to re-oxidation of reduced inorganic compounds (Rasmussen and
228 Jørgensen, 1992; Canfield et al., 2005).

229 Total anaerobic C_{org} mineralization rates were determined by linear regression of the
230 accumulation of total DIC with time during the anoxic bag incubations (Fig. 3) after
231 correcting for $CaCO_3$ precipitation (Thamdrup et al., 2000). Briefly, $CaCO_3$ precipitation was
232 calculated from decreasing dissolved Ca^{2+} concentration during the anoxic bag incubation:

233

$$234 \Delta CaCO_3 = \Delta [Ca^{2+}]_{sol} \times (1 + K_{Ca}) \quad (2)$$

235

236 where, K_{Ca} is the adsorption constant for Ca^{2+} ($K_{Ca} = 1.6$) (Li and Gregory, 1974). Then the
237 DIC production rate corrected for $CaCO_3$ precipitation was calculated as:

238

$$239 \text{DIC production} = \text{DIC accumulation} + CaCO_3 \text{ precipitation} \quad (3)$$

240

241 Fe(III) reduction rates were determined by linear regression of the increase in solid-phase
242 Fe(II)_(oxal) content with time during anoxic bag incubations. The dissimilatory microbial
243 Fe(III) reduction rate was derived by subtracting abiotic Fe reduction coupled to the
244 oxidation of sulfide produced by sulfate reduction (Gribsholt et al., 2003):

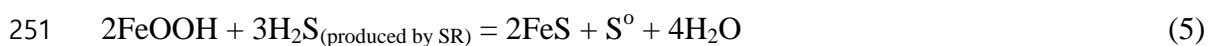
245

$$246 \text{Dissimilatory microbial Fe(III) Red} = \text{Total Fe(III) Red} - \text{Abiotic Fe(III) Red} \quad (4)$$

247

248 assuming that abiotic Fe reduction coupled to H_2S oxidation occurred at a stoichiometry of 2
249 Fe(III) per 3 H_2S (Pyzik and Sommer, 1981; Melton et al., 2014):

250

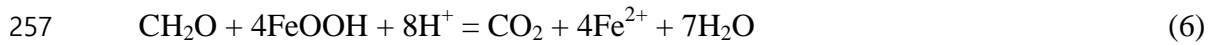


252

253 Finally, to estimate the C_{org} oxidation by microbial Fe reduction, the 4:1 stoichiometry of

254 iron reduction coupled to C_{org} oxidation was used from the stoichiometric equation (Canfield
255 et al., 1993a):

256



258

259 Mn reduction rates were determined from linear regression of the production of dissolved
260 Mn^{2+} with time during the anoxic bag incubations. Similar to previous studies (e.g., Canfield
261 et al., 1993a, 1993b; Thamdrup and Dalsgaard, 2000), we assumed that accumulating
262 dissolved Mn was Mn^{2+} . This ignores a potential contribution from Mn^{3+} , which in some
263 cases can constitute a substantial fraction of the dissolved Mn pool at the upper boundary of
264 the zone with soluble Mn accumulation in marine sediments (Madison et al., 2013). Further
265 studies of the dynamics of soluble Mn^{3+} are required to evaluate its potential importance in
266 anoxic incubations. Such studies pending, we find justification for our assumption in the
267 good agreement observed in the previous studies between Mn reduction rates calculated
268 based on the assumption that soluble Mn is Mn^{2+} (Eq. 7) and independent estimates of rates
269 of carbon mineralization through dissimilatory Mn reduction based on DIC or NH_4^+
270 accumulation. Due to strong adsorption of Mn^{2+} to Mn oxide surfaces (Canfield et al., 1993b),
271 the Mn reduction rates were estimated after compensating for the adsorption effect of Mn^{2+} to
272 Mn-oxides according to Thamdrup and Dalsgaard (2000):

273

$$274 \quad \text{Mn reduction rate} = \text{Mn}^{2+} \text{ accumulation rate} \times (1 + K_{\text{Mn}}^{*2+} \times (1 - \Phi) \times \Phi^{-1} \times \delta_s) \quad (7)$$

275

276 where, Φ = porosity

277 δ_s = density of sediment

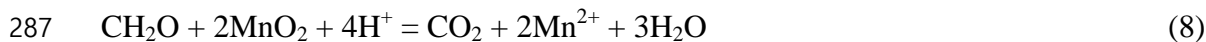
$$278 \quad K_{\text{Mn}}^{*2+} = 4.8 + 0.14 \times [\text{Mn(IV)}] \text{ (ml g}^{-1}\text{)}$$

$$279 \quad [\text{Mn(IV)}] = \text{the content of Mn(IV) (}\mu\text{mol g}^{-1}\text{)}$$

280

281 We here assume that extracted $\text{Mn}_{(\text{DCA})}$ represents Mn(IV) as observed in surface
282 sediments of another Mn-rich site (Canfield et al., 1993b; Thamdrup and Dalsgaard, 2000).
283 Small levels of $\text{Mn}_{(\text{DCA})}$ remaining at depth further suggest that little Mn(II) accumulates in
284 the solid phase (*see* Results). C_{org} oxidation by dissimilatory Mn(IV) reduction was
285 calculated from the stoichiometric equation (Canfield et al., 1993a):

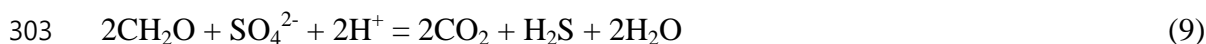
286



288

289 Sulfate reduction rates were determined using the radiotracer method of Jørgensen (1978).
290 Sediment cores (35 cm long with 2.9 cm i.d.) were collected in triplicate, injected
291 horizontally at 1-cm vertical interval with 5 μL radiolabeled sulfate ($^{35}\text{S}\text{-SO}_4^{2-}$, 15 kBq μL^{-1} ,
292 Amersham) diluted in sterilized NaCl solution (3.0 %), and incubated for 12 h at *in situ*
293 temperature. At the end of the incubation, the sediment was sliced into sections, fixed in Zn
294 acetate (20 %), and frozen at $-25\text{ }^\circ\text{C}$ until processed in the laboratory. The reduced ^{35}S was
295 recovered using distillation with a boiling acidic Cr^{2+} solution according to Fossing and
296 Jørgensen (1989). Background radioactivity of ^{35}S was $32.4 \pm 3.7\text{ cpm cm}^{-3}$ ($n = 10$) at site
297 D3 and $87.5 \pm 38.7\text{ cpm cm}^{-3}$ ($n = 10$) at site M1. Detection limits of the SRR, estimated from
298 the double standard deviation of the blank value (i.e., 7.4 and 77.4 cpm) according to Fossing
299 et al. (2000), ranged from 0.79 to 2.62 $\text{nmol cm}^{-3}\text{ d}^{-1}$. To elucidate the contribution of sulfate
300 reduction in anaerobic carbon oxidation, the SRRs (Fig. 5B, 5G) were converted to carbon
301 oxidation using a stoichiometric equation (Thamdrup and Canfield, 1996):

302



304

305 **3 Results**

306

307 **3.1 Pore-water and solid-phase constituents**

308

309 The depth distributions of NH_4^+ , NO_3^- , Mn^{2+} and Fe^{2+} in the pore-water as well as solid phase
310 Mn, Fe and S for the two stations are shown in Fig. 2. NH_4^+ concentrations at M1 increased
311 steadily with depth (Fig. 2A) whereas at D3 it decreased down to 3 cm depth before it
312 increased below (Fig. 2F). Highest concentrations of nitrate were measured at 0 to 1 cm
313 sediment depth at the two stations and concentrations decreased below a background level ($<$
314 2 μM) below 1 cm at both M1 and D3 (Fig. 2A, 2F). Dissolved Mn^{2+} concentrations differed
315 widely between the sites showing a maximum of 56 μM between 0 and 3 cm depth and not
316 exceeding 10 μM below at M1 (Fig. 2B), whereas at D3 concentrations increased to a
317 maximum of 286 μM at 10–12 cm depth (Fig. 2G). Conversely, dissolved Fe^{2+} concentrations

318 at M1 increased from 11 μM at 0–0.5 cm to 32 μM at 6–7 cm depth, and stayed constant
319 below (Fig. 2C), whereas at D3, concentrations were uniformly low showing a slight increase
320 to 12 μM at 15 cm (Fig. 2H).

321 Extractable Mn ($\text{Mn}_{(\text{DCA})}$) contents were low ($< 3 \mu\text{mol cm}^{-3}$) in the upper 20 cm at the
322 slope site (M1) (Fig. 2B), but up to 200 $\mu\text{mol cm}^{-3}$ in the upper 4 cm depth of the sediment at
323 the center of the basin (D3), with a sharp decrease to near depletion ($\sim 1 \mu\text{mol cm}^{-3}$) below 10
324 cm (Fig. 2G). At the slope site (M1), contents of $\text{Fe}(\text{III})_{(\text{oxal})}$ decreased slightly with
325 increasing depth from 28 $\mu\text{mol cm}^{-3}$ near the surface to 13 $\mu\text{mol cm}^{-3}$ at 20 cm depth,
326 mirroring an increase in $\text{Fe}(\text{II})_{(\text{oxal})}$ (Fig. 2D). At the center of the basin (D3), $\text{Fe}(\text{III})_{(\text{oxal})}$
327 increased slightly from 67 $\mu\text{mol cm}^{-3}$ at 0–0.5 cm to 90 $\mu\text{mol cm}^{-3}$ at 4–6 cm depth, and
328 decreased steeply below to 4.8 $\mu\text{mol cm}^{-3}$ at 12–14 cm depth (Fig. 2I). Of total $\text{Fe}_{(\text{oxal})}$,
329 $\text{Fe}(\text{III})_{(\text{oxal})}$ comprised $> 98 \%$ at 0–2 cm and $> 97 \%$ at 0–8 cm depth at M1 and D3,
330 respectively. The fraction of $\text{Fe}(\text{III})_{(\text{oxal})}$ in $\text{Fe}_{(\text{oxal})}$ then decreased to 40 % at 10–12 cm depth
331 at both sites. Acid volatile sulfur (AVS) exhibited a slight increase with depth at M1 from 0.8
332 $\mu\text{mol cm}^{-3}$ at the surface to 7.2 $\mu\text{mol cm}^{-3}$ at 20 cm depth (Fig. 2E), but was not detected at
333 D3 (Fig. 2J). Chromium reducible sulfur (CRS) contents at M1 increased rapidly with depth
334 from 1.9 $\mu\text{mol cm}^{-3}$ at 0–0.5 cm to 21.8 $\mu\text{mol cm}^{-3}$ at 20 cm depth (Fig. 2E), whereas the
335 CRS contents remained $< 0.1 \mu\text{mol cm}^{-3}$ at D3 (Fig. 2J).

336

337 **3.2 O₂ microprofiles and diffusive oxygen uptake rate**

338

339 Oxygen penetrated less than 4 mm into the sediments (Fig. 3), and rates of diffusive oxygen
340 uptake (DOU) were 7.1 and 6.0 $\text{mmol O}_2 \text{ m}^{-2} \text{ d}^{-1}$ at M1 and D3, respectively (Table 2).
341 Oxygen consumption by aerobic respiration estimated from the O₂ micro-profiles (area I and
342 II in Fig. 3) was higher at the M1 in the slope site ($4.0 \text{ mmol O}_2 \text{ m}^{-2} \text{ d}^{-1}$) than at the D3 in the
343 center of the basin ($2.5 \text{ mmol O}_2 \text{ m}^{-2} \text{ d}^{-1}$). O₂ consumption by re-oxidation of reduced
344 inorganic compounds indicated by increased activity at the oxic/anoxic interface (area III in
345 Fig. 3) accounted for 43 % and 57 % of the DOU at M1 and D3, respectively. From the
346 profiles of geochemical constituents (Fig. 2), O₂ consumption was mainly attributed to the re-
347 oxidation of sulfide and Fe^{2+} at M1 and of Mn^{2+} at D3.

348

349 **3.3 Anoxic bag incubations**

350

351 Changes in concentrations of DIC, Ca^{2+} and dissolved Mn^{2+} and solid $\text{Fe(II)}_{(\text{oxal})}$ contents
352 over time during anoxic bag incubations from sediment of 0–2, 2–4, 4–6 and 6–8 cm depth
353 intervals are presented in Fig. 4. The DIC concentrations increased linearly over time during
354 incubations of sediment in all bags from M1 and D3, except the bag from 6–8 cm at D3. The
355 DIC accumulation rates were generally higher at the slope site (M1) than at the basin site (D3)
356 (Table 4). The concentrations of Ca^{2+} decreased with time at all depth intervals of M1,
357 whereas a decrease of Ca^{2+} was observed only for the 2–4 cm depth interval at D3. The
358 decrease of Ca^{2+} indicates CaCO_3 precipitation, which consequently underestimates DIC
359 accumulation, especially at M1.

360 Coinciding with high solid $\text{Mn}_{(\text{DCA})}$ contents (Fig. 2G), prominent Mn^{2+} accumulation
361 appeared at 0–6 cm depth of D3, whereas no increase of Mn^{2+} was observed at M1 except a
362 slight accumulation at 0–2 cm interval (Fig. 4). Solid $\text{Fe(II)}_{(\text{oxal})}$ contents increased linearly
363 with time at 0–4 cm depth of M1, whereas highest $\text{Fe(II)}_{(\text{oxal})}$ accumulation was observed at
364 4–6 cm depth at D3. An increase of $\text{Fe(II)}_{(\text{oxal})}$ was not discernible in the Mn-oxide-rich
365 surface sediment (0–2 cm) of D3.

366

367 **3.4 Sulfate reduction rates (SRR)**

368

369 At the slope site (M1), SRR increased from $18 \text{ nmol cm}^{-3} \text{ d}^{-1}$ at the surface to $97\text{--}103 \text{ nmol}$
370 $\text{cm}^{-3} \text{ d}^{-1}$ at 1.5–2 cm depth, and decreased below to $12.5 \text{ nmol cm}^{-3} \text{ d}^{-1}$ at 20 cm depth (Fig.
371 5B). In contrast, SRR at the manganese oxide-rich basin site (D3) ranged from 1.7 to 8.7
372 $\text{nmol cm}^{-3} \text{ d}^{-1}$, and did not vary with depth (Fig. 5G). Depth integrated SRR down to 10 cm
373 depth was 10 times higher at M1 ($4.3 \text{ mmol m}^{-2} \text{ d}^{-1}$) than at D3 ($0.4 \text{ mmol m}^{-2} \text{ d}^{-1}$) (Table 3).

374

375 **3.5 DIC production rates**

376

377 Vertical profiles of the DIC production rate that were derived from the linear regression of
378 the DIC production measured in anoxic bag incubation (Fig. 4) after correcting for CaCO_3
379 precipitation, are presented in Fig. 5C and 5H for M1 and D3, respectively. At M1, the DIC
380 production rates decreased with depth from $280 \text{ nmol cm}^{-3} \text{ d}^{-1}$ (0–2 cm depth) to 69 nmol cm^{-3}
381 d^{-1} (8–10 cm depth) (Fig. 5C), whereas the DIC production rates at D3 were relatively
382 similar across the upper 6 cm ranging from 86 to $136 \text{ nmol cm}^{-3} \text{ d}^{-1}$, and decreased to 8–15
383 $\text{nmol cm}^{-3} \text{ d}^{-1}$ at 6–10 cm (Fig. 5H). The integrated DIC production rate within 10 cm depth

384 of the sediment was twice as high at M1 ($14.0 \text{ mmol m}^{-2} \text{ d}^{-1}$) as at the D3 ($7.2 \text{ mmol m}^{-2} \text{ d}^{-1}$)
385 (Table 4).

386

387 **3.6 Rates of Mn and Fe reduction**

388

389 The accumulation of Mn^{2+} presented evidence that manganese reduction was occurring in the
390 surface sediment (0–6 cm) of D3 (Fig. 4). The manganese reduction rate (MnRR) derived
391 from Mn^{2+} accumulation with correction for adsorption ranged from $7.5 \text{ nmol cm}^{-3} \text{ d}^{-1}$ (0–2
392 cm depth) to $198 \text{ nmol cm}^{-3} \text{ d}^{-1}$ (2–4 cm depth) at D3 (Fig. 5I). In contrast, MnRR at M1 was
393 indiscernible except for low activity ($2.2 \text{ nmol cm}^{-3} \text{ d}^{-1}$) at 0–2 cm depth (Fig. 5D). Depth
394 integrated MnRR at D3 ($8.21 \text{ mmol m}^{-2} \text{ d}^{-1}$) was 200 times higher than the MnRR at M1
395 ($0.04 \text{ mmol m}^{-2} \text{ d}^{-1}$) (Table 3). The iron reduction rate (FeRR), derived from $\text{Fe(II)}_{(\text{oxal})}$
396 accumulation, at M1 was highest in the 0–2 cm interval ($237 \text{ nmol cm}^{-3} \text{ d}^{-1}$), and then
397 decreased with depth to $38 \text{ nmol cm}^{-3} \text{ d}^{-1}$ at 8–10 cm depth (Fig. 5E). In contrast, Fe
398 reduction was not detected in the surface sediment at D3, but increased to its maximum rate
399 of $240 \text{ nmol cm}^{-3} \text{ d}^{-1}$ at 4–6 cm depth. The FeRR then decreased with depth to 12 nmol cm^{-3}
400 d^{-1} at 8–10 cm (Fig. 5J) where a few data points were adopted to derive the line of best-fit
401 regression. Depth integrated total FeRR was slightly higher at M1 ($11.4 \text{ mmol m}^{-2} \text{ d}^{-1}$) than at
402 D3 ($7.53 \text{ mmol m}^{-2} \text{ d}^{-1}$) (Table 3). The ratio of microbial Fe reduction, $\text{Fe Red}_{(\text{microbial})}$, to
403 abiotic Fe reduction coupled to sulfide oxidation, $\text{Fe Red}_{(\text{abiotic})}$, ranged from 1.14 (8–10 cm at
404 M1) to 52.3 (2–4 cm at D3), which indicated that the Fe reduction at Mn- and Fe oxides rich
405 basin site was mostly a microbiologically mediated process (Table 3).

406

407 **4 Discussion**

408

409 **4.1 Partitioning of C_{org} oxidation in accordance with the distribution of terminal** 410 **electron acceptors**

411

412 One of the most prominent features revealed from the vertical distributions of geochemical
413 constituents at the basin site (D3) was that electron acceptors such as O_2 , nitrate, Mn- and Fe
414 oxides were systematically distributed with discrete zonation according to the order of
415 decreasing energy yield for C_{org} oxidation (Fig. 5F). Such biogeochemical zones are not
416 sharply separated in most aquatic sediments due to, e.g., sediment heterogeneity and mixing

417 resulting from bioirrigation, bioturbation, and bottom turbidity currents. The profiles of
418 dissolved and solid phase geochemical constituents in the sediment provide indications as to
419 specific diagenetic reactions prevailing (Froelich et al., 1979). However, reoxidation of
420 reduced inorganic compounds often mask the primary reactions involved in carbon oxidation
421 (Sørensen and Jørgensen, 1987; Hines et al., 1991). Together with the discrete geochemical
422 zonation of the electron acceptors, the independently executed metabolic rate measurements
423 (Fig. 5) allowed us to evaluate the relative contribution of each terminal electron-accepting
424 pathway with sediment depth.

425 Previous experimental studies that have quantified pathways of anaerobic carbon
426 oxidation in subtidal marine sediments have generally determined the contributions of Mn
427 and Fe reduction indirectly from the difference between rates of DIC production and sulfate
428 reduction converted to carbon equivalents (e.g., Canfield et al., 1993b; Thamdrup and
429 Canfield, 1996; Vandieken et al., 2006). The inferred rates of Mn and Fe reduction were
430 further supported by the depth distribution of metal oxides and patterns of Mn^{2+} and Fe^{2+}
431 accumulation in the pore water, but could not be verified because the accumulation of
432 particulate Mn(II) and Fe(II) – which represents the overwhelming fraction of the reduced
433 pools – was not quantified. Here, we combined the indirect approach with independent
434 determination of Mn and Fe reduction rates. Thus, we obtained two separate estimates of
435 anaerobic carbon oxidation rates; based on DIC production and on the sum of sulfate, Fe, and
436 Mn reduction converted to carbon equivalents, respectively (Table 4). At M1, within the 0–10
437 cm depth interval, the average ratio between total anaerobic C_{org} oxidation rate ($10.7 \text{ mmol C m}^{-2} \text{ d}^{-1}$)
438 and the C_{org} oxidation from DIC production ($14.0 \text{ mmol C m}^{-2} \text{ d}^{-1}$) was 0.77 (Table 4).
439 Similarly, at D3, the average ratio between total anaerobic C_{org} oxidation ($6.79 \text{ mmol m}^{-2} \text{ d}^{-1}$)
440 and anaerobic DIC production ($7.22 \text{ mmol m}^{-2} \text{ d}^{-1}$) was 0.94. There was a good agreement
441 between the two estimates with a ratio of total anaerobic C_{org} oxidation by Mn + Fe + sulfate:
442 DIC production for individual depth intervals of 0.8–1.2 (Table 4) with the exception at the
443 0–2 cm depth of slope site (M1) where the ratio was slightly lower, 0.66, possibly due to a
444 contribution from the C_{org} oxidation by nitrate reduction. The similarity of the two estimates
445 across all incubations spanning a range of redox conditions provides confidence in our
446 approach for calculating dissimilatory Mn and Fe reduction rates. Specifically, the good
447 agreement indicates that the underlying assumptions concerning Mn adsorption and reactions
448 of Fe(III) and sulfide are valid as first-order approximations. The general agreement further
449 supports the validity of previous determinations of dissimilatory Mn and Fe reduction rates

450 based on the difference between DIC production and SO_4^{2-} reduction (Canfield et al., 1993a,
451 1993b; Thamdrup et al., 2000; Vandieken et al., 2006; Vandieken et al., 2014).

452 To elucidate the contribution of sulfate reduction in anaerobic carbon oxidation, the SRRs
453 (Fig. 5B, 5G) were converted to carbon oxidation (Thamdrup and Canfield, 1996), and then
454 compared to the DIC production rates from anoxic bag incubation (Fig. 5C, 5H). At the slope
455 site (M1), the fraction of anaerobic C_{org} oxidation coupled to sulfate reduction increased with
456 depth from 48 % at 0–2 cm, to 80 % at 8–10 cm (Table 4). Thus, the excess C_{org} oxidation in
457 the upper layers should be coupled to other electron accepting processes. Indeed, the C_{org}
458 oxidation by Fe reduction ($0.96 \text{ mmol m}^{-2} \text{ d}^{-1}$) accounted for most of the remaining anaerobic
459 C_{org} oxidation (12–18 % of DIC production) at 0–8 cm depth, consistent with the distribution
460 of Fe(III) decreasing from $> 25 \mu\text{mol cm}^{-3}$ near the surface (Fig. 6, Table 4). Mn reduction
461 was of minor importance at M1 because of the low content of Mn oxide ($< 3 \mu\text{mol cm}^{-3}$).
462 Carbon oxidation coupled to aerobic respiration was estimated to $3.1 \text{ mmol m}^{-2} \text{ d}^{-1}$
463 corresponding to 18 % of the total aerobic + anaerobic oxidation, while the contributions of
464 Fe and sulfate reduction to this total were 12 % and 50 %, respectively (Table 4). As
465 mentioned above, nitrate reduction/denitrification may contribute part of the unexplained 19 %
466 of carbon oxidation, but most of this imbalance likely reflects the combined uncertainties in
467 the estimates of the individual pathways. Additionally, our partitioning of carbon oxidation
468 pathways could be biased towards the anaerobic electron acceptors due to the use of the
469 diffusive oxygen uptake (DOU) rather than total oxygen uptake (TOU), which will exceed
470 DOU if bioirrigation is active (Glud, 2008). Bioirrigation was not determined at our sites, but
471 the pore water profiles show no indication of strong irrigation (Fig. 2). An average
472 DOU/TOU ratio of ~ 0.6 has been reported for sediments at 1.5–2.5 km depth (Glud, 2008).
473 Using this ratio, and assuming that TOU is partitioned similarly as DOU between aerobic
474 carbon oxidation and reoxidation, aerobic carbon oxidation would account for 25 %, while Fe
475 and sulfate reduction would account for 11 % and 46 % of of carbon oxidation, respectively.
476 This, the potential bias from using DOU is not expected to affect the ranking of electron
477 acceptors by quantitative importance ($\text{SO}_4^{2-} > \text{O}_2 > \text{Fe(III)}$), and, as discussed further below,
478 the partitioning of C_{org} oxidation at M1 falls within the range previously reported for
479 continental margin sediments.

480 In contrast to M1, C_{org} oxidation by sulfate reduction at the basin site (D3) accounted for
481 only a small fraction ($< 11 \%$) of anaerobic C_{org} oxidation at 0–6 cm interval and it only
482 dominated carbon oxidation at 8–10 cm (Fig. 5H, Table 4). Oxygen and NO_3^- were depleted

483 within 3.6 mm and 1 cm depth of the sediment surface, respectively (Fig. 5F), while Mn and
484 Fe(III) oxides were abundant at 0–4 cm and 0–6 cm, respectively. Consistent with the
485 abundance of electron acceptors, high rates of Mn and Fe reduction (Fig. 5I and 5J) implied
486 Mn and Fe reduction as the most significant C_{org} oxidation pathways to 6 cm depth. At 0–2
487 cm depth, C_{org} oxidation by aerobic respiration and Mn reduction accounted for 53 % and 43 %
488 of total C_{org} oxidation, respectively (Fig. 6). At 2–4 cm, Mn reduction accounted for 73 % of
489 total C_{org} oxidation and 92 % of anaerobic C_{org} oxidation (Table 4, Fig. 6). Its importance
490 decreased to 22 % at 4–6 cm due to lower Mn contents, while microbial Fe(III) reduction
491 here contributed 51 %, and the partitioning of sulfate reduction increased to 11 % (Fig. 6).
492 Consequently, the relative distribution of each C_{org} oxidation pathway with depth at D3 (Fig.
493 6) matched well with the depth distribution of the respective electron acceptors (Fig. 5F).
494 Overall, within the 10 cm depth sediment interval, Mn and Fe reduction were the dominant
495 C_{org} oxidation pathways comprising 45 % and 20 % of total carbon oxidation, respectively, at
496 the Mn and Fe oxide-rich site in the center of the UB (Table 4). Correction for a potential
497 underestimation of TOU, as discussed for M1, would reduce the contributions of Mn and Fe
498 reduction slightly to 41 % and 18 %, respectively.

499 Despite the high Fe oxide content at 0–4 cm at D3 (Fig. 5F), no solid Fe(II)_(oxal)
500 accumulation was observed at this depth range (Fig. 4). This indicates that Fe(III) reduction
501 may not occur under these Mn-oxide rich conditions. Indeed, using a combination of 16S
502 rRNA-stable isotope probing and geochemical analysis in three manganese oxides-rich
503 sediments including the UB, Vandieken et al. (2012) identified bacteria related to *Colwellia*,
504 *Oceanospillaceae* and *Arcobacter* as acetate-oxidizing bacteria that potentially reduce
505 manganese, whereas no known iron reducers were detected in the Mn-rich sediment.
506 Similarly, Thamdrup et al. (2000), in Mn oxide-rich Black Sea sediment, found that the
507 abundance of viable Fe-reducing bacteria in most probable number counts was low in
508 comparison to Mn reducers and the addition of ferrihydrite did not stimulate Fe reduction,
509 which implied that Fe reduction should be outcompeted by the Mn reduction process.

510 As manganese reduction is thermodynamically more favorable than iron and sulfate
511 reduction, the Mn²⁺ liberation (Fig. 4) is likely resulted from dissimilatory Mn reduction.
512 Nonetheless, Mn reduction estimated from the increase of Mn²⁺ at 0–4 cm interval at D3 (Fig.
513 4) could be due to oxidation of Fe²⁺ or sulfide. Fe²⁺ may readily react with Mn oxides (Myers
514 and Nealson, 1988; Lovley and Phillips, 1988) by the reaction $2\text{Fe}^{2+} + \text{MnO}_2 + 4\text{H}_2\text{O} = \text{Mn}^{2+}$
515 $+ 2\text{Fe}(\text{OH})_3 + 2\text{H}^+$. However, in the Mn oxide-rich sediment of the Skagerrak, Canfield et al.

516 (1993b) revealed that the addition of Ferrozine, a strong complexation agent for Fe^{2+} , had no
517 inhibitory effect on the Mn^{2+} liberation, indicating that the chemical reaction of MnO_2 with
518 Fe^{2+} generated by Fe reduction was not responsible for the accumulation of Mn^{2+} .

519 Despite the anoxic conditions and nitrate depletion during the bag incubation, Mn
520 reduction rates at 0–2 cm depth (Fig. 5I) based on Mn^{2+} accumulation were substantially
521 lower than the rates inferred from DIC accumulation (Fig. 5H). A similar discrepancy was
522 previously observed for the uppermost part of the Mn reduction zone (Thamdrup et al., 2000),
523 and is likely explained by particularly strong sorption of Mn^{2+} to fresh Mn oxide surfaces,
524 which is not included in the adsorption coefficient used here. Low Mn^{2+} together with the
525 rapid decrease of nitrate at 0–2 cm depth at D3 (Fig. 2F, 2G) also suggested that dissolved
526 reduced manganese might act as a reducing agent for nitrate as it was suggested by Aller et al.
527 (1998) in the Panama Basin and Mogollón et al. (2016) in the deep-sea sediment of the
528 Clarion-Clerton fracture zone in the northeast equatorial Pacific.

529 Previous estimation of denitrification in 0–2 cm depth of the UB ranged from 0.01 to 0.17
530 $\text{mmol N m}^{-2} \text{d}^{-1}$ (Lee, 2009), which is equivalent to a C_{org} oxidation of 0.013–0.213 mmol C
531 $\text{m}^{-2} \text{d}^{-1}$ using the stoichiometric equation of $4\text{H}^+ + 5\text{CH}_2\text{O} + 4\text{NO}_3^- = 5\text{CO}_2 + 2\text{N}_2 + 7\text{H}_2\text{O}$.
532 Based on the average, the contribution of carbon oxidation by denitrification (0.11 mmol C
533 $\text{m}^{-2} \text{d}^{-1}$) should be minor at the basin site ($\leq 3\%$ of total C_{org} oxidation at 0–2 cm; $\sim 1\%$ of
534 integrated C_{org} oxidation). This is consistent with the general consensus that C_{org} oxidation by
535 denitrification is of little importance in most marine sediments (Sørensen et al., 1979;
536 Canfield et al., 1993a; Trimmer and Engström, 2011). Denitrification may be even further
537 suppressed in Mn-rich sediments due to competitive inhibition from Mn reduction (Trimmer
538 et al., 2013).

539

540 **4.2 C_{org} oxidation dominated by manganese reduction in the UB**

541

542 Microbial Fe reduction has been quantified directly in sediments of various coastal oceans
543 (Gribsholt et al., 2003; Kostka et al., 2002a, 2002b; Hyun et al., 2007, 2009b) and indirectly
544 in deeper continental margins (Thamdrup and Canfield, 1996; Jensen et al., 2003; Kostka et
545 al., 1999). Earlier estimation from 16 different continental margin sediments indicated that
546 Fe(III) reduction contributed 22 % on average to anaerobic carbon oxidation (Thamdrup,
547 2000). Thus, the contributions from Fe(III) reduction of 12 % and 20 % of anaerobic C_{org}
548 oxidation on the slope (M1) and in the basin (D3) of the UB (Table 4) fall in the range of the

549 previous indirect estimates.

550 Unlike Fe reduction, direct estimation of manganese reduction rates is not easy, mainly
551 because of the restriction of the process to a thin surface layer (Sundby and Silverberg, 1985),
552 the rapid reduction of manganese oxides with H_2S and Fe^{2+} (Postma, 1985; Burdige and
553 Nealson, 1986; Kostka et al., 1995; Lovley and Phillips, 1988), and the adsorption of Mn^{2+} to
554 Mn oxide surface (Canfield et al., 1993b). For that reason, only two studies, from the
555 Skagerrak and Black Sea, are available for direct comparison on the partitioning of Mn
556 reduction. The process has also been indicated to be of importance in the Panama Basin based
557 on diagenetic modeling (Aller, 1990) and at some Arctic shelf sites where it was however not
558 quantified separately from Fe reduction (Vandieken et al., 2006; Nickel et al., 2008). Mn
559 reduction was responsible for over 90 % of total C_{org} oxidation at 600 m depth in the
560 Skagerrak (Canfield et al., 1993b), and accounted for 13–45 % of anaerobic C_{org} oxidation in
561 the Black Sea shelf sites at 60–130 m of water depth (Thamdrup et al., 2000). To our
562 knowledge, this report of C_{org} oxidation dominated by Mn reduction comprising 45 % of total
563 C_{org} oxidation and 57 % of anaerobic C_{org} respiration in the center of the UB (Table 4)
564 represents the first from deep-offshore basin of the eastern Asian marginal seas.

565 The difference in partitioning of Mn reduction in C_{org} oxidation between the UB, Black
566 Sea and Skagerrak reflects the close relationship between Mn oxide content in the sediment
567 and Mn reduction (Thamdrup et al., 2000). From the vertical distribution of electron
568 acceptors (Fig. 5F) and contribution of each C_{org} oxidation pathway with depth (Fig. 6), it is
569 apparent that the availability of Mn(IV) largely controls the relative contribution to C
570 oxidation. In the Skagerrak, the Mn oxides are abundant in high content down to 10 cm depth
571 (Canfield et al., 1993b), whereas Mn oxides in the Black Sea and the Ulleung Basin were
572 enriched only down to 2 cm and 4 cm, respectively (Thamdrup et al., 2000; Fig. 2G). Using
573 the available data set for the three marine sediments, we further plotted the relative
574 contribution of manganese reduction to anaerobic carbon oxidation as a function of Mn-
575 oxides content to expand data from Thamdrup (2000) (Fig. 7). The plot indicates saturation
576 kinetics with a close correlation between Mn oxide content and the importance of Mn
577 reduction at low contents. Curve-fitting yields a content of MnO_2 at 50 % of contribution of
578 manganese reduction to total C_{org} oxidation (K_s) of $8.6 \mu\text{mol cm}^{-3}$ similar to the approx. 10
579 $\mu\text{mol cm}^{-3}$ suggested before (Thamdrup et al., 2000). This indicates that Mn reduction can be
580 a dominant C_{org} oxidation process even at low contents of Mn oxides compared to those
581 found at UB. Manganese enrichments of this magnitude have been reported for several

582 locations on the continental margins and in deep basins (Murray et al., 1984; Gingele and
583 Kasten, 1994; Gobeil et al., 1997; Haese et al., 2000; Mouret et al., 2009; Magen et al., 2011;
584 Macdonald and Gobeil, 2012; Mewes et al., 2014) in addition to the relatively few places
585 where dissimilatory Mn reduction was already indicated to be of importance, as discussed
586 above. Thus, the process may be of more widespread significance, particularly in deep basin
587 settings such as UB that allow geochemical focusing of manganese.

588

589 **4.3 Source of high Mn oxide content**

590

591 The strong enrichment of Mn in the UB surface sediment is primarily of diagenetic origin as
592 indicated by just slightly higher Mn contents at depth in the sediment at D3 (mean $1.1 \mu\text{mol}$
593 cm^{-3} at 10–20 cm depth) compared to M1 ($0.45 \mu\text{mol cm}^{-3}$) (Fig. 2) combined with higher
594 sediment accumulation rates at the slope ($0.15\text{--}0.3 \text{ cm y}^{-1}$) than in the basin (0.07 cm y^{-1} ; Cha
595 et al., 2005). Thus, the burial flux of Mn, and thereby the net input assuming steady state
596 deposition, is similar or higher at M1 compared to D3. Furthermore, Mn is likely subject to
597 geochemical focusing in the basin as Mn depositing at shallower depths is reductively
598 mobilized and incompletely oxidized in the thin oxic surface layer, resulting in release to the
599 water column and net down-slope transport, as inferred in other ventilated basins (Sundby
600 and Silverberg, 1985; Canfield et al., 1993b; Schaller and Wehrli, 1997). A diagenetic source
601 of Mn enrichment was also concluded in previous studies (Yin et al., 1989; Cha et al., 2007;
602 Choi et al., 2009). The Mn remaining and being buried at M1 likely represents unreactive
603 detrital forms to a larger extent than at D3 (Cha et al., 2007). Adopting the sediment
604 accumulation rate of 0.07 cm y^{-1} in the UB determined at a station 50 km from D3 (Cha et al.,
605 2005), the average $\text{Mn}_{(\text{DCA})}$ content of $1.1 \mu\text{mol cm}^{-3}$ at 10–20 cm depth (Fig. 2G)
606 corresponds to a flux for permanent burial of $0.002 \text{ mmol m}^{-2} \text{ d}^{-1}$ or just 0.03 % of the Mn
607 reduction rate (Table 3), i.e., an Mn atom is recycled 3800 times before it finally gets buried
608 – first by stripping from the particles that settle to the seafloor and subsequently, over and
609 over, by reductive dissolution of the Mn oxides that form by reoxidation in the oxic surface
610 layer (or, potentially, in the nitrate zone; Aller et al., 1998; Mogollón et al., 2016). This is a
611 much more extensive recycling than found in the Mn sediment of Skagerrak (130–260 times;
612 Canfield et al., 1993b). The difference results mainly from a much higher burial flux of Mn
613 (as authigenic Mn[II]) in the Skagerrak ($\sim 40 \mu\text{mol cm}^{-3}$; Canfield et al., 1993b). The reason
614 that little, if any, authigenic Mn(II) is buried in the UB is not clear.

615 As noted in previous studies (Aller, 1990; Canfield et al., 1993b), high contributions of Mn
616 and Fe reduction to carbon oxidation in off-shore sediments requires physical mixing, which
617 typically occurs through bioturbation. This is also the case for the UB, where the burial flux
618 from the oxic surface layer into the Mn reduction zone corresponded to $0.4 \text{ mmol m}^{-2} \text{ d}^{-1}$ or 5 %
619 of the Mn reduction rate ($213 \text{ } \mu\text{mol cm}^{-3} \times 0.07 \text{ cm y}^{-1}$). Bioturbation has previously been
620 inferred, but not quantified, from ^{210}Pb profiles in the UB (Cha, 2002), and thin polychaete
621 worms were observed during our sampling. Assuming bioturbation to be a diffusive process,
622 we estimate, in a similar manner as in the previous studies and based on the average gradient
623 in $\text{Mn}_{(\text{DCA})}$ from 0.5–1 to 7–8 cm, that the Mn reduction rate would be supported at a
624 biodiffusion coefficient of $9.5 \text{ cm}^2 \text{ y}^{-1}$. This value is 3.6 times lower than the coefficient
625 estimated for the Skagerrak (Canfield et al., 1993b) and consistent with estimates for other
626 sediments with similar deposition rates (Boudreau, 1994). The estimated biodiffusion
627 coefficient (Db) of $9.5 \text{ cm}^2 \text{ yr}^{-1}$ at Site D3 corresponds to ~2 % of the molecular diffusion
628 coefficient of oxygen ($388 \text{ cm}^2 \text{ yr}^{-1}$). Judging from the absence of major fauna in the UB
629 sediments, the mixing is brought about by small organisms with each individual affecting
630 only a small area relative to the size of our cores, and the Db averaging many of these small
631 and local but frequent events. Under such conditions, bioturbation can drive Mn cycling in
632 the UB without substantial smearing of the redox zonation. Similarly, Hyacinthe et al. (2001)
633 found that well defined profiles can be observed in both sediments with low and high
634 bioactivity in the Bay of Biscay.

635

636 **4.4 The UB as a biogeochemical hotspot**

637

638 The SRRs measured in this study ($0.43\text{--}4.29 \text{ mmol m}^{-2} \text{ d}^{-1}$) are higher than those measured in
639 productive systems such as the Benguela upwelling system in the Southeast Atlantic (0.14--
640 $1.39 \text{ mmol m}^{-2} \text{ d}^{-1}$; Ferdelman et al., 1999), and even comparable to those reported at the
641 Chilean ($2.7\text{--}4.8 \text{ mmol m}^{-2} \text{ d}^{-1}$; Thamdrup and Canfield, 1996) and Peruvian ($5.2 \text{ mmol m}^{-2} \text{ d}^{-1}$;
642 Fossing, 1990) upwelling system at a similar depth range of 1000–2500 m. The total
643 anaerobic DIC production rates at the slope ($14.0 \text{ mmol m}^{-2} \text{ d}^{-1}$) and basin site (7.2 mmol m^{-2}
644 d^{-1}) were also comparable to those measured at the same depth range of a Chilean upwelling
645 site ($9.2\text{--}11.6 \text{ mmol m}^{-2} \text{ d}^{-1}$) (Thamdrup and Canfield, 1996). Since rates of benthic carbon
646 oxidation are largely controlled by the supply of C_{org} (Canfield et al., 2005), a high C_{org} flux

647 reflected in the high C_{org} content (> 2.5 %, dry wt.) in the sediment of the UB (Table 1) is
648 likely to explain the high metabolic activities. A similar high C_{org} content as in the UB is
649 rarely found in deep-sea sediment underlying oxic bottom water at depths exceeding 2000 m,
650 except for a Chilean upwelling site (Lee et al., 2008). This high C_{org} content in the UB is
651 mainly associated with the combination of enhanced biological production resulting from the
652 formation of coastal upwelling (Hyun et al., 2009a), enhanced new production in summer
653 (Kwak et al., 2013), occurrence of an intrathermocline eddy resulting in the extraordinary
654 subsurface chlorophyll-a maximum (Kim et al., 2012), high C_{org} accumulation rates
655 exceeding $2 \text{ g C m}^{-2} \text{ yr}^{-1}$ (Lee et al., 2008), and high export production (Kim et al., 2009).
656 Consequently, high benthic mineralization resulting from the high C_{org} in the sediment
657 implied that the UB is a biogeochemical hotspot where significant turnover of organic matter
658 and nutrient regeneration occur.

659 Recent oceanographic observations revealed that the gradual deoxygenation and warming
660 of the bottom water of the East Sea over the last 30 years have resulted in an ~ 10 %
661 decrease in dissolved oxygen and ~ 0.04 °C increase in potential temperature (Kim et al.,
662 2001; Gamo et al., 2011). Benthic metabolism and respiratory C_{org} oxidation coupled to
663 various terminal electron-accepting processes in the sediments are largely controlled by the
664 combination of O_2 content, temperature and biological production overlying water column
665 (Canfield et al., 2005). It is thus important to monitor any changes in the rates and
666 partitioning of C_{org} oxidation to better understand and predict the variations of
667 biogeochemical cycles of carbon, nutrients and metals potentially associated with long-term
668 climatic changes in the UB, the biogeochemical hotspot of the East Sea.

669

670 **5. Conclusions**

671

672 Surface sediments of the Ulleung Basin (UB) in the East Sea are characterized by a high C_{org}
673 content (> 2.5 %, dry wt.), high contents of Fe oxides (up to $100 \mu\text{mol cm}^{-3}$), and very high
674 contents of Mn oxides ($> 200 \mu\text{mol cm}^{-3}$). We show that microbial Mn and Fe reduction are
675 the dominant C_{org} oxidation pathways, comprising 45 % and 20 % of total C_{org} oxidation,
676 respectively. The high Mn content results from highly efficient recycling through reoxidation
677 with very low permanent burial of authigenic Mn(II) phases. The basin topography may
678 ensure that any Mn^{2+} escaping to the overlying water returns to the sediment after
679 reprecipitation. The relative importance of Mn reduction to C_{org} oxidation displays saturation

680 kinetics with respect to Mn oxide content with a low half-saturation value ($8.6 \mu\text{mol cm}^{-3}$),
681 which further implies that Mn reduction can be a dominant C_{org} oxidation process in
682 sediments with lower MnO_2 content, and thereby that the process might be more important in
683 continental margin and deep basin sediments than previously thought. Vertical distributions
684 of the major terminal electron acceptors such as O_2 , nitrate, Mn- and Fe oxides were
685 systematically zoned with discrete sequential depletion according to the order of decreasing
686 energy yield for C_{org} oxidation, which are not sharply separated in most aquatic sediments
687 due to, e.g., sediment heterogeneity and mixing resulting from bioirrigation, bioturbation, and
688 bottom turbidity currents. High benthic mineralization resulting from the high C_{org} content in
689 the sediment implied that the UB is a biogeochemical hotspot where significant turnover of
690 organic matter and nutrient regeneration occur.

691

692 **Author contribution**

693

694 J-H Hyun as first author and leader of the Korean research group designed the original
695 experiments and conducted most writing; S-H Kim, J-S Mok, and H Cho participated in
696 onboard research activities and analytical processes; V Vandieken participated in onboard
697 research and was actively involved in the discussion of the manuscript; T Lee, as project
698 manager of the EAST-1 program, paid the ship-time and has participated in discussion of the
699 results; B Thamdrup, as leader of the Danish research group, collaborated with J-H Hyun in
700 designing the experiments and writing and discussing the manuscript.

701

702 **Acknowledgements**

703

704 This research was a part of the projects titled Korean Long-term Marine Ecological
705 Researches (K-LTMER) and Deep Water Circulation and Material Cycling in the East Sea
706 (EAST-II) funded by the Korean Ministry of Oceans and Fisheries, and was also supported by
707 the National Research Foundation of Korea (NRF-2012-013-2012S1A2A1A01030760) in
708 collaboration with the Danish Council for Independent Research and the Danish National
709 Research Foundation (DNRF53). The authors thank Dr. S. Pantoja (handling editor), Dr. S.
710 Kasten and two anonymous reviewers for their comments that improved the earlier version of
711 the manuscript.

712

713 **References**

714

715 Aller, R. C. : Bioturbation and manganese cycling in hemipelagic sediments, Phil. Trans. R.
716 Soc. Lond. A 331, 51-68, 1990.

717 Aller, R. C., Hall, P. O. J., Rude, P. D., and Aller, J. Y. : Biogeochemical heterogeneity and
718 suboxic diagenesis in hemipelagic sediments of the Panama Basin, Deep-Sea Res. I, 45,
719 133-165, 1998.

720 Belkin, I. M. : Rapid warming of Large Marine Ecosystems, Prog. Oceanogr., 81, 207-213,
721 2009.

722 Berg, P., Risgaard-Petersen, N., and Rysgaard, S. : Interpretation shelf and slope: A
723 comparison of *in situ* microelectrode and chamber flux measurements, Limnol. Oceanogr.,
724 37, 614-629, 1998.

725 Boudreau, B. P. : Is burial velocity a master parameter for bioturbation?, Geochim.
726 Cosmochim. Acta, 58, 1243-1249, 1994.

727 Bowles, M. W., Mogollón, J. M., Kasten, S., Zabel, M., and Hinrichs, K.U. : Global rates of
728 marine sulfate reduction and implications for sub-sea-floor metabolic activities, Science,
729 344, 889-891, 2014.

730 Broecker, W. S. : The great ocean conveyor, Oceanogr., 4, 79-89, 1991.

731 Broecker, W. S. and Peng, T. H. : Tracers in the sea, Lamont-Doherty Earth Observatory,
732 Palisades, NY., 1982.

733 Burdige, D. J. and Nealson, K. H. : Chemical and microbiological studies of sulfide-mediated
734 manganese reduction, Geomicrobiol. J., 4, 361-387, 1986.

735 Canfield, D. E., Jørgensen, B. B., Fossing, H., Glud, R., Gundersen, J., Rasing, N. B.,
736 Thamdrup, B., Hansen, J. W., Nielsen, L. P., and Hall, P. O. J. : Pathways of organic
737 carbon oxidation in three continental margin sediments, Mar. Geol., 113, 27-40, 1993a.

738 Canfield, D. E., Thamdrup, B., and Hansen, J. W. : The anaerobic degradation of organic
739 matter in Danish coastal sediments: iron reduction, manganese reduction, and sulfate
740 reduction, Geochim. Cosmochim. Acta, 57, 3867-3883, 1993b.

741 Canfield, D. E., Thamdrup, B., and Kristensen, E. (Eds.) : Aquatic geomicrobiology, Elsevier,
742 San Diego, 640 pp., 2005.

743 Cha, H. J., Choi, M. S., Lee, C.-B., and Shin, D.-H. : Geochemistry of surface sediments in
744 the southwestern East/Japan Sea, J. Asian Earth Sci., 29, 685-697, 2007.

745 Cha, H. J., Lee, C. B., Kim, B. S., Choi, M. S., and Ruttenger, K. C. : Early diagenetic

746 redistribution and burial of phosphorus in the sediments of the southwestern East Sea
747 (Japan Sea), *Mar. Geol.*, 216, 127-143, 2005.

748 Cha, H. J. : Geochemistry of surface sediments and diagenetic redistribution of phosphorus in
749 the southwestern East Sea, PhD thesis, Seoul National Univ., Seoul, Korea, 190 pp., 2002.

750 Choi, Y. J., Kim, D. S., Lee, T. H., and Lee, C. B. : Estimate of manganese and iron oxide
751 reduction rates in slope and basin sediments of Ulleung Basin, East Sea, *J. Korean Soc.*
752 *Oceanogr.*, 14, 127-133, 2009.

753 Chough, S. K., Lee, H. J., and Yoon, S. H. (Eds.) : *Marine Geology of Korean Seas* (2nd
754 edition), Elsevier, Amsterdam, 2000.

755 Cline, J. D. : Spectrophotometric determination of hydrogen sulfide in natural waters, *Limnol.*
756 *Oceanogr.*, 14, 454-458, 1969.

757 D'Hondt, S., Inagaki, F., Zarikian, C. A., Abrams, L. J., Dubois, N., Engelhardt, T., Evans,
758 H., Ferdelman, T., Gribsholt, B., Harris, R. N., Hoppie, B. W., Hyun, J.-H. et al. :
759 Presence of oxygen and aerobic communities from sea floor to basement in deep-sea
760 sediments, *Nature Geosci.*, 8, 299-304, 2015.

761 Ferdelman, T. G., Fossing, H., Neumann, K., and Schulz, H. D. : Sulfate reduction in surface
762 sediments of the southeast Atlantic continental margin between 15°38'S and 27°57'S
763 (Angola and Namibia), *Limnol. Oceanogr.*, 44, 650-661, 1999.

764 Fossing, H., Ferdelman, T. G., and Berg, P. : Sulfate reduction and methane oxidation in
765 continental margin sediments influenced by irrigation (South-East Atlantic off Namibia),
766 *Geochim. Cosmochim. Acta*, 64, 897-910, 2000.

767 Fossing, H. and Jørgensen, B. B. : Measurement of bacterial sulfate reduction in sediments:
768 evaluation of a single-step chromium reduction method, *Biogeochem.*, 8, 205-222, 1989.

769 Froelich, P. N., Klinkhammer, G.P., Bender, M.L., Luedtke, N.A., Heath, G.R., Cullen, D.,
770 Dauphin, P., Hammond, D., Hartman, B., and Maynard, V. : Early oxidation of organic
771 matter in pelagic sediments of the eastern equatorial Atlantic: suboxic diagenesis,
772 *Geochim. Cosmochim. Acta*, 43, 1075-1090, 1979.

773 Gamo, T. : Dissolved oxygen in the bottom water of the Sea of Japan as a sensitive alarm for
774 global climatic change, *Trend Anal.Chem.*, 30, 1308-1319, 2011.

775 Gamo, T., Nakayama, N., Takahata, N., Sano, Y., Zhang, J., Yamazaki, E., Taniyasu, S., and
776 Yamashita, N. : The Sea of Japan and its unique chemistry revealed by time-series
777 observations over the last 30 Year, *Monogr. Environ. Earth Planets*, 2, 1-22, 2014.

778 Gingele, F. X. and Kasten, S. : Solid-phase manganese in Southeast Atlantic sediments

779 Implications for the paleoenvironment, *Mar. Geol.*, 121, 317-332, 1994.

780 Glud, R. N. : Oxygen dynamics of marine sediments, *Mar. Biol. Res.*, 4, 243-289, 2008.

781 Gobeil, C, Macdonald, R. W., and Sundby, B. : Diagenetic separation of cadmium and
782 manganese in suboxic continental margin sediments, *Geochim. Cosmochim. Acta*, 61,
783 4647-4654, 1997.

784 Gribsholt, B., Kostka, J. E., and Kristensen, E. : Impact of fiddler crabs and plant roots on
785 sediment biogeochemistry in a Georgia saltmarsh, *Mar. Ecol. Prog. Ser.*, 259, 237-251,
786 2003.

787 Haese, R. R., Schramm, J., Rutgers Van Der Loeff, M. M., and Schulz, H. D. : A
788 comparative study of iron and manganese diagenesis in continental slope and deep
789 sea basin sediments off Uruguay (SW Atlantic), *Int. J. Earth Sci.*, 88, 619-629, 2000.

790 Hall, P. O. and Aller, R.C. : Rapid small-volume, flow injection analysis for CO₂ and NH₄⁺ in
791 marine and freshwaters, *Limnol. Oceanogr.*, 37, 113-119, 1992.

792 Hansen, C., Zabel, M., and Schulz, H. N. : Benthic cycling of oxygen, nitrogen, and
793 phosphorus, in: *Marine Geochemistry*, edited by: Schulz, H. D. and Zabel, M., Springer-
794 Verlag, Berlin, Heidelberg, NY, 207-240, 2006.

795 Hansen, J. W., Thamdrup, B., and Jørgensen, B. B. : Anoxic incubation of sediment in gas-
796 tight plastic bags: a method for biochemical process studies, *Mar. Ecol. Prog. Ser.*, 208,
797 273-282, 2000.

798 Hines, M. E., Bzylinski, D. A., Tugel, J. B., and Lyons, W. B. : Anaerobic microbial
799 biogeochemistry in sediments from two basins in the Gulf of Maine: evidence for iron and
800 manganese reduction, *Estuar. Coast. Shelf Sci.*, 32, 313-324, 1991.

801 Hyacinthe, C., Anschutz, P., Carbonel, P., Jouanneau, J.-M., Jorissen, F.J. : Early diagenetic
802 processes in the muddy sediments of the Bay of Biscay, *Mar. Geol.*, 177, 111-128, 2001.

803 Hyun, J.-H., Kim, D., Shin, C.-W., Noh, J.-H., Yang, E.-J., Mok, J.-S., Kim, S.-H., Kim, H.-
804 C., and Yoo, S. : Enhanced phytoplankton and bacterioplankton production coupled to
805 coastal upwelling and an anticyclonic eddy in the Ulleung basin, East Sea, *Aquat. Microb.*
806 *Ecol.*, 54, 45-54, 2009a.

807 Hyun, J.-H., Mok, J.-S., Cho, H.-Y., Kim, S.-H., and Kostka, J. E. : Rapid organic matter
808 mineralization coupled to iron cycling in intertidal mud flats of the Han River estuary,
809 Yellow Sea, *Biogeochem.*, 92, 231-245, 2009b.

810 Hyun, J.-H., Mok, J.-S., You, O.-R., Kim, D., and Choi, D. L.: Variations and controls of
811 sulfate reduction in the continental slope and rise of the Ulleung basin off the southeast
812 Korean upwelling system in the East Sea, *Geomicrobiol. J.*, 27, 1-11, 2010.

813 Hyun, J.-H., Smith, A. C., and Kostka, J. E. : Relative contributions of sulfate- and iron(III)
814 reduction to organic matter mineralization and process controls in contrasting habitats of
815 the Georgia saltmarsh, *Appl. Geochem.*, 22, 2637-2651, 2007.

816 Jahnke, R. A., Reimers, C. E., and Craven, D. B. : Intensification of recycling of organic
817 matter at the sea floor near ocean margins, *Nature*, 348, 50-54, 1990.

818 Jahnke, R. A. and Jahnke, D. B. : Rates of C, N, P and Si recycling and denitrification at the
819 US mid-Atlantic continental slope depocenter, *Deep-Sea Res. I*, 47, 1405-1428, 2000.

820 Jahnke, R. A., Emerson, S. R., and Murray, J. W. : A model of oxygen reduction,
821 denitrification, and organic matter mineralization in marine sediments, *Limnol. Oceanogr.*,
822 27, 610-623, 1982.

823 Jensen, M. M., Thamdrup, B., Rysgaard, S., Holmer, M., and Fossing, H. : Rates and
824 regulation of microbial iron reduction in sediments of the Baltic-North Sea transition,
825 *Biogeochem.*, 65, 295-317, 2003.

826 Jørgensen, B. B. and Kasten, S. : Sulfur cycling and methane oxidation. in: *Marine*
827 *Geochemistry*, edited by: Schulz, H. D. and Zabel, M., Springer-Verlag, Berlin,
828 Heidelberg, NY, 271-309, 2006.

829 Jørgensen, B. B. : A comparison of methods for the quantification of bacterial sulfate
830 reduction in coastal marine sediments, 1. Measurement with radiotracer techniques,
831 *Geomicrobiol. J.*, 1, 11-28, 1978.

832 Jørgensen, B. B. : Bacteria and marine biogeochemistry, in: *Marine Geochemistry*, edited by:
833 Schulz, H. D. and Zabel, M., Springer-Verlag, Berlin, Heidelberg, NY, 169-206, 2006.

834 Jørgensen, B. B. : Mineralization of organic matter in the sea bed - the role of sulphate
835 reduction, *Nature*, 296, 643-645, 1982.

836 Jørgensen, B. B. and Revsbech, N. P. : Diffusive boundary layers and the oxygen uptake of
837 sediments and detritus, *Limnol. Oceanogr.*, 30, 111-122, 1985.

838 Kang, D. J., Lee, D. S., and Kim, K.-R. : The East Sea (Sea of Japan), in: *Carbon and nutrient*
839 *fluxes in continental margins*, edited by: Liu, K.-K., Atkinson, L., Quiñones, R. A., and
840 Talaue-MaManus, L., Springer-Verlag, Berlin, Heidelberg, 383-394, 2010.

841 Kim K, Kim K.-R., Min, D. H., Volkov, Y., Yoon, J.-H., Takematsu, M. : Warming and
842 structural changes in the East Sea (Japan) Sea: a clue to future changes in the global

843 oceans?, *Geophys. Res. Lett.*, 28, 3293-3296, 2001.

844 Kim, D., Choi, M.-S., Oh, H.-Y., Kim, K. H., and Noh, J.-H. : Estimate of particulate organic
845 carbon export flux using $^{234}\text{Th}/^{238}\text{U}$ disequilibrium in the southwestern East Sea during
846 summer, (*The Sea*) *J. Kor. Soc. Oceanogr.*, 14, 1-9, 2009.

847 Kim, D., Yang, E.J., Kim, K. H., Shin, C.-W., Park, J., Yoo, S. J., and Hyun, J.-H. : Impact of
848 an anticyclonic eddy on the summer nutrient and chlorophyll a distributions in the Ulleung
849 Basin, East Sea (Japan Sea), *ICES J. Marine Science*, 69, 23-29, 2012.

850 Kostka, J. E., Gribsholt, B., Petrie, E., Dalton, D., Skelton, H., and Kristensen, E. : The rates
851 and pathways of carbon oxidation in bioturbated saltmarsh sediments, *Limnol.Oceanogr.*,
852 47, 230-240, 2002a.

853 Kostka, J. E., Roychoudhury, A., and Van Cappellen, P. : Rates and controls of anaerobic
854 microbial respiration across spatial and temporal gradients in saltmarsh sediments,
855 *Biogeochem*, 60, 49–76, 2002b.

856 Kostka, J. E., Thamdrup, B., Glud, R. N., and Canfield, D. E. : Rates and pathways of carbon
857 oxidation in permanently cold Arctic sediments, *Mar. Ecol. Prog. Ser.*, 180, 7-21, 1999.

858 Kostka, J. E., Luther, G. W., and Neelson, K. H. : Chemical and biological reduction of
859 Mn(III)-pyrophosphate complexes – potential importance of dissolved Mn(III) as an
860 environmental oxidant, *Geochim. Cosmochim. Acta*, 59, 885-894, 1995.

861 Kwak, J. H., Hwang, J., Choy, E. J., Park, H. J., Kang, D.-J., Lee, T., Chang, K.-I. Kim, K.-R.,
862 and Kang, C.-K.: High primary productivity and f-ratio in summer in the Ulleung Basin of
863 the East/Japan Sea, *Deep-Sea Res. Pt. I*, 79, 74–85, 2013.

864 Lee, J.: Importance of nitrate reduction in coastal and deep-sea sediments, MS thesis,
865 Department of Marine Science Graduate School, Pusan National University, Korea, 86 pp.,
866 2009.

867 Lee, T., Hyun, J.-H., Mok, J. S., and Kim, D. : Organic carbon accumulation and sulfate
868 reduction rates in slope and basin sediments of the Ulleung basin, East/Japan Sea, *Geo.*
869 *Mar. Lett.* 28, 153-159, 2008.

870 Li, Y. H. and Gregory, S. : Diffusion of ions in sea water and deep sea sediments. *Geochim.*
871 *Cosmochim. Acta*, 38, 703-714, 1974.

872 Liu, K.-K., Atkinson, L., Quiñones, R. A., and Talaue-MaManus, L. : Biogeochemistry of the
873 continental margins, in: *Carbon and nutrient fluxes in continental margins*, edited by: Liu,
874 K.-K., Atkinson, L., Quiñones, R. A., and Talaue-MaManus, L., Springer-Verlag, Berlin,
875 Heidelberg, 3-24, 2010.

876 Lovley, D. R. and Phillips, E. J. P. : Competitive mechanisms for inhibition of sulfate
877 reduction and methane production in the zone of ferric iron reduction in sediments, *Appl.*
878 *Environ. Microbiol.*, 53, 2636-2641, 1987.

879 Lovley, D. R. and Phillips, E. J. P. : Manganese inhibition of microbial iron reduction in
880 anaerobic sediments, *Geomicrobiol. J.*, 6, 145-155, 1988.

881 Luther III, G. W. : Acid volatile sulfide – A comment, *Mar. Chem.*, 97, 198-205, 2005.

882 Macdonald, R. W. and Gobeil, C. : Manganese sources and sinks in the Arctic Ocean with
883 reference to periodic enrichments in basin sediments, *Aquat. Geochem.*, 18, 565-591, 2012.

884 Madison, S., Tebo, B. M., Mucci, A., Sundby, B., and Luther III, G. W. : Abundant
885 porewater Mn(III) is a major component of the sedimentary redox system, *Science*, 341,
886 875-878, 2013.

887 Magen, C., Mucci, A., and Sundby, B. : Reduction rates of sedimentary Mn and Fe oxides: an
888 incubation experiment with Arctic Ocean sediments, *Aquat. Biogeochem.*, 17, 629-643,
889 2011.

890 Melton, E. D., Swanner, E. D., Behrens, S., Schmidt, C., and Kappler, A. : The interplay of
891 microbially mediated and abiotic reactions in the biogeochemical Fe cycle, *Nature Rev.*
892 *Microbiol.*, 12, 797-808, 2014.

893 Mewes, K., Mogollón, J. M., Picard, A., Rühlemann, C., Eisenhauer, A., Kuhn, T., Ziebis, W.,
894 and Kasten, S. : Diffusive transfer of oxygen from seamount basaltic crust into overlying
895 sediments: an example from the Clarion-Clipperton Fracture Zone, *Earth Planet. Sci. Lett.*,
896 433, 215-225, 2016.

897 Mewes, K., Mogollón, J. M., Picard, A., Rühlemann, C., Kuhn, T., Nöthen, K., and Kasten,
898 S. : Impact of depositional and biogeochemical processes on small scale variations in
899 nodule abundance in the Clarion-Clipperton Fracture Zone, *Deep-Sea Res. I*, 91, 125-141,
900 2014.

901 Meyers, C. and Nealson, K. H. : Microbial reduction of manganese oxides: Interactions with
902 iron and sulfur, *Geochim. Cosmochim. Acta*, 52, 2727-2732, 1988.

903 Mogollón, J. M., Mewes, K., and Kasten, S. : Quantifying manganese and nitrogen cycle
904 coupling in manganese-rich, organic carbon-starved marine sediments: examples from the
905 Clarion-Clipperton fracture zone, *Geophys. Res. Lett.*, 43, doi:10.1002/2016GL069117,
906 2016.

907 Mouret, A., Anschutz, P., Lecroart, P., Chaillou, G., Hyacinthe, C., Deborde, J., Jorissen,
908 F., Deflandre, B., Schmidt, S., and Jouanneau, J.-M. : Benthic geochemistry of manganese

909 inthe Bayof Biscay, and sediment mass accumulation rate, *Geo. Mar. Lett.* 29, 133-149,
910 2009.

911 Murray, J. W., Balistrieri, L. S., and Paul, B. : The oxidation stateof manganese in
912 marinesediments and ferromanganesenodules, *Geochim. Cosmochim. Acta*, 48, 1237-
913 1247, 1984.

914 Nickel, M., Vandieken, V., Brüchert, V., and Jørgensen, B. B. : Microbial Mn(IV) and Fe(III)
915 reduction in northern Barents Sea sediments under different conditions of ice cover and
916 organic carbon deposition, *Deep-Sea Res. II*, 55, 2390-2398, 2008.

917 Parsons, T. R., Maita, Y., and Lalli, C. M.(Eds.) : A manual of chemical and biological
918 methods for seawater analysis, Pergamon Press, Oxford, 173 pp., 1984.

919 Phillips, E. J. P.and Lovley, D. R. : Determination of Fe(III) and Fe(II) in oxalate extracts of
920 sediment, *Soil Sci. Soc. Am. J.*, 51, 938-941, 1987.

921 Postma, D. : Concentration of Mn and separation from Fe in sediments – I. Kinetics and
922 stoichiometry of the reaction between birnessite and dissolved Fe(II) at 10°C, *Geochim.*
923 *Cosmochim. Acta*, 49, 1023-1033, 1985.

924 Pyzik, A. E.and Sommer, S. E. : Sedimentary iron monosulfide: kinetics and mechanisms of
925 formation, *Geochim. Cosmochim. Acta*, 45, 687-698, 1981.

926 Rasmussen, H. and Jørgensen, B. B. : Microelectrode studies of seasonal oxygen uptake in a
927 coastal sediment: role of molecular diffusion, *Mar. Ecol. Prog. Ser.*, 81, 289-303, 1992.

928 Rickard, D. and Morse, J. W. : Acid volatile sulfur (AVS), *Mar. Chem.*, 97, 141-107, 2005.

929 Romankevich, E. A. : *Geochemistry of organicmatter in the ocean*, Springer-Verlag, Berlin,
930 Heidelberg, NY, Tokyo, 334 pp., 1984.

931 Schaller, T. and Wehrli, B. : Geochemical-focusing of manganese in lake sediments –An
932 indicator of deep-water oxygen conditions, *Aquat. Geochem.*, 2, 359-378, 1997.

933 Slomp, C. P., Mort, H. P., Jilbert, T., Reed, D. C., and Gustafsson, B. G. : Coupled dynamics
934 of iron and phosphorus in sediments of an oligotrophic coastal basin and the impact of
935 anaerobic oxidation of methane, *PLoS ONE*, 8, e62386, 2013.

936 Sørensen, J. W. and Jørgensen, B. B. : Early diagenesis in sediments from Danish coastal
937 waters: Microbial activity and Mn-Fe-S geochemistry, *Geochim. Cosmochim. Acta*, 51,
938 1583-1590, 1987.

939 Sørensen, J. W., Jørgensen, B. B., and Revsbech, N. P. : A comparison of oxygen, nitrate and
940 sulfate respiration in a coastal marine sediment, *Microb. Ecol.*, 5, 105-115, 1979.

941 Stookey, L. L. : Ferrozine - a new spectrophotometric reagent for iron, *Anal. Chemi.* 42, 779-

942 781, 1970.

943 Sundy, B. and Silverberg, N. : Manganese fluxes in the benthic boundary layer, *Limnol.*
944 *Oceanogr.*, 30, 372-381, 1985.

945 Thamdrup, B. and Canfield, D. E. : Pathways of carbon oxidation in continental margin
946 sediments off central Chile, *Limnol. Oceanogr.* 41, 1629-1650, 1996.

947 Thamdrup, B. and Dalsgaard, T. : The fate of ammonium in anoxic manganese oxide-rich
948 marine sediment, *Geochim. Cosmochim. Acta*, 64, 4157-4164, 2000.

949 Thamdrup, B., Rosselló-Mora, R., and Amann, R. : Microbial manganese and sulfate
950 reduction in Black Sea shelf sediments, *Appl. Environ. Microbiol.*, 66, 2888-2897, 2000.

951 Thamdrup, B. : Bacterial manganese and iron reduction in aquatic sediments, *Adv. Microb.*
952 *Ecol.* 16, 41-84, 2000.

953 Trimmer, M. and Engström, P. : Distribution, activity, and ecology of anammox bacteria in
954 aquatic environments, in: *Nitrification*, edited by: Ward, B. B., Arp, D. J., and Klotz, M. G.,
955 ASM Press, Washington, DC, 201-235, 2011.

956 Trimmer, M., Engström, P., and Thamdrup, B. : Stark contrast in denitrification and anammox
957 across the deep Norwegian Trench in the Skagerrak, *Appl. Environ. Microbiol.*, 79, 7381-
958 7389, 2013.

959 Vandieken, V., Pester, M., Finke, N., Hyun, J.-H., Friedrich, M. W., Loy, A., and Thamdrup,
960 B. : Identification of acetate-oxidizing manganese-reducing bacteria in three manganese
961 oxide-rich marine sediments by stable isotope probing, *ISME J.*, 6, 2078-2090, 2012.

962 Vandieken, V., Finke, N., and Thamdrup, B. : Hydrogen, acetate, and lactate as electron
963 donors for microbial manganese reduction in a manganese-rich coastal marine sediment,
964 *FEMS Microbiol Ecol.*, 87, 733-745, 2014.

965 Vandieken, V., Nickel, M., and Jørgensen, B. B. : Carbon mineralization in Arctic sediments
966 northeast of Svalbard: Mn(IV) and Fe(III) reduction as principal anaerobic respiratory
967 pathways, *Mar. Ecol. Prog. Ser.*, 322, 15-27, 2006.

968 Walsh, J. J. : Importance of continental margins in the marine biogeochemical cycling of
969 carbon and nitrogen, *Nature*, 350, 53-55, 1991.

970 Yamada, K., Ishizaka, J., and Nagata, H. : Spatial and temporal variability of satellite primary
971 production in the Japan Sea from 1998 to 2002, *J. Oceanogr.*, 61, 857-869, 2005.

972 Yin, J. H., Kajiwara, Y., and Fujii, T. : Distribution of transition elements in surface
973 sediments of the southwestern margin of Japan Sea. *Geochem. J.*, 23, 161-180, 1989.

974 Yoo, S. and Park, J. S. : Why is the southwest the most productive region of the East Sea/Sea
975 of Japan?, J. Mar. Syst., 78, 301-315, 2009.

976

977 Table 1. Environmental settings and sediment characteristics

Environmental parameter	M1 (Continental slope)	D3 (Center of the basin)
Latitude	36° 10' N	37° 00' N
Longitude	130° 10' E	131° 00' E
Water depth (m)	1,453	2,154
Sediment temperature (°C)	1.3	0.6
Pore-water salinity (psu)	34.2	34.8
Water content (%)	85 (± 3.1)	77 (± 1.8)
Porosity	0.95 (± 0.03)	0.86 (± 0.01)
Density (g cm ⁻³)	1.10 (± 0.02)	1.12 (± 0.02)
Total organic carbon (% , dry wt.)	3.96 (± 0.27)	2.66 (± 0.09)
Total nitrogen (% , dry wt.)	0.38 (± 0.01)	0.35 (± 0.01)

978 Numbers in parenthesis indicate ± 1SD of triplicate samples.

979

980

981
982
983
984

Table 2. Oxygen penetration depth (OPD), diffusive oxygen utilization (DOU) rate and O₂ consumption rate by aerobic respiration and re-oxidation of reduced inorganic compounds (RIC) in the pore water.

Station	OPD (mm)	DOU (mmol O ₂ m ⁻² d ⁻¹)	O ₂ consumption (mmol O ₂ m ⁻² d ⁻¹) by	
			Aerobic respiration	Re-oxidation of RIC
M1	3.2 (± 0.20)	7.12 (± 1.36)	4.04 (± 2.03)	3.07 (± 0.68)
D3	3.6 (± 0.03)	5.95 (± 0.16)	2.53 (± 0.72)	3.42 (± 0.58)

985
986
987
988

Values represent averages ± 1SD (*n* = 3)

989 Table 3. Depth integrated rates ($\text{mmol m}^{-2} \text{d}^{-1}$) of Mn reduction, Fe reduction, and sulfate reduction and the partitioning of abiotic and microbial Fe(III) reduction in total
 990 Fe(III) reduction with depth.

St.	Depth Interval (cm)	SO_4^{2-} Red	Mn Red	^(a) Total Fe(III) Red	Fe reduction by		Fe Red _(Microbial) / Fe Red _(Abiotic)
					^(a) Abiotic Fe Red	^(a) Microbial Fe Red	
M1	0–2	1.35	0.04	4.75	0.90	3.86	4.28
	2–4	1.04	-	3.02	0.70	2.33	3.33
	4–6	0.84	-	1.58	0.56	1.21	2.16
	6–8	0.54	-	1.25	0.36	0.89	2.47
	8–10	0.53	-	0.77	0.36	0.41	1.14
	Sum (0-10)	4.30	0.04	11.4	2.88	8.70	
D3	0–2	0.06	^(b) 3.19	-	-	-	n.a.
	2–4	0.11	3.96	1.63	0.07	1.56	22.3
	4–6	0.13	1.05	4.80	0.09	4.71	52.3
	6–8	0.06	0.01	0.86	0.04	0.83	20.8
	8–10	0.07	0.00	0.24	0.05	0.19	3.80
	Sum (0-10)	0.43	8.21	7.53	0.25	7.29	

991 ^(a)Stoichiometric equations were used to evaluate the relative significance of abiotic and microbial Fe reduction:

992 Abiotic reduction of Fe(III) by sulfide oxidation, $3\text{H}_2\text{S} + 2\text{FeOOH} = 2\text{FeS} + \text{S}^0 + 4\text{H}_2\text{O}$; Microbial Fe(III) reduction = Total Fe(III) reduction – abiotic Fe(III) reduction.

993 ^(b)back-calculated from the C oxidation by Mn reduction in the 0–2 cm interval in Table 4 using the stoichiometric equation, $2\text{MnO}_2 + \text{CH}_2\text{O} + \text{H}_2\text{O} = 2\text{Mn}^{2+} + \text{HCO}_3^- + 3\text{OH}^-$.

994 ‘–’ indicates that the process does not occur or is regarded as negligible at the depth interval based on the OPD for aerobic respiration and geochemical profiles or anoxic
 995 bag incubations for Mn(IV) and Fe(III) reduction

996 ‘n.a.’ indicates that data are not available.

997

998

999

Table 4. Organic carbon (C_{org}) oxidation ($mmol C m^{-2} d^{-1}$) by each C_{org} oxidation pathway, and its partitioning in total C_{org} oxidation (% Total C_{org} ox) and anaerobic C_{org} oxidation (% Anaerobic C_{org} ox) at each depth interval within 10 cm of the sediment. Mn Red, Mn reduction; Fe Red, Fe reduction; and SO_4^{2-} Red, sulfate reduction

St.	Depth Interval (cm)	C_{org} oxidation measured by		^(c) Total C_{org} oxidation (DOU + DIC)	Anaerobic C_{org} oxidation by dissimilatory			Total anaerobic C_{org} oxidation (Mn Red + Fe Red + SO_4^{2-} Red)	Total Anaerobic C_{org} oxidation / Anoxic DIC production	
		^(a) DOU (Aerobic respiration)	^(b) DIC prod. (Anaerobic respiration)		^(d) Mn Red	^(d,e) Fe Red	^(d) SO_4^{2-} Red			
M1	0–2	3.11	5.59	8.70	0.02	0.96	2.69	3.67	0.66	
	2–4	-	3.31	3.31	-	0.58	2.09	2.67	0.81	
	4–6	-	2.26	2.26	-	0.26	1.67	1.93	0.85	
	6–8	-	1.50	1.50	-	0.22	1.08	1.30	0.87	
	8–10	-	1.37	1.37	1.37	-	0.10	1.06	1.17	0.85
	Sum (0–10)	3.11	14.0	17.1	0.02	2.13	8.59	10.7	0.77	
	(% Total C_{org} ox) (% Anaerobic C_{org} ox)	(18.1)	(81.9)	(100)	(0.13)	(12.4)	(50.1)	(62.7)		
D3	0–2	1.94	1.72	3.66	^(f) 1.59	-	0.13	1.72	1.00	
	2–4	-	2.72	2.72	1.98	0.39	0.22	2.58	0.95	
	4–6	-	2.32	2.32	0.52	1.18	0.26	1.96	0.84	
	6–8	-	0.30	0.30	0.01	0.21	0.12	0.33	1.10	
	8–10	-	0.16	0.16	0.16	-	0.05	0.19	1.21	
	Sum (0–10)	1.94	7.22	9.2	4.10	1.82	0.86	6.79	0.94	
	(% Total C_{org} ox) (% Anaerobic C_{org} ox)	(20.6)	(78.8)	(100)	(44.8)	(19.9)	(9.41)	(77.8)		

1000
1001
1002
1003
1004
1005
1006
1007
1008
1009
1010

^(a) Aerobic C_{org} oxidation rate (= O_2 consumption by aerobic respiration \times (106C/138 O_2) calculated using the Redfield ratio; O_2 consumption by aerobic respiration rate (= DOU - re-oxidation rates) is calculated from Table 2 that is derived from the O_2 micro-profiles in Fig. 2.

^(b) independently measured from the DIC accumulation rate in anoxic bag incubation experiment in Fig. 4.

^(c) Total C_{org} oxidation = aerobic C_{org} oxidation + anaerobic C_{org} oxidation

^(d) C_{org} oxidation by dissimilatory Mn(IV) reduction, Fe(III) reduction, and sulfate reduction was calculated from the stoichiometric equations: $2MnO_2 + CH_2O + H_2O = 2Mn^{2+} + HCO_3^- + 3OH^-$; $4Fe(OH)_3 + CH_2O = 4Fe^{2+} + HCO_3^- + 7OH^-$; $SO_4^{2-} + 2CH_2O = H_2S + 2HCO_3^-$; $H_2S = HS^- + H^+$

^(e) Dissimilatory Fe(III) reduction = (Total Fe(III) reduction in Fig. 5) – (Abiotic Fe(III) reduction coupled to H_2S oxidation; $3H_2S + 2FeOOH = 2FeS + S^0 + 4H_2O$)

^(f) back-calculated from: DIC production rate - (C oxidation by SO_4^{2-} Red and Fe Red). See text for further discussion

‘ - ’ indicates that the process does not occur or is regarded as negligible based on the OPD for aerobic respiration and geochemical profiles or anoxic bag incubations for Mn and Fe Red.

Figure legends

Fig. 1. Sampling stations in the East Sea and pictures showing contrasting colors between surface sediments of the continental slope (M1) and center of the basin (D3)

Fig. 2. Concentrations of dissolved NH_4^+ , NO_3^- , Mn^{2+} and Fe^{2+} in pore water and contents of solid phase $\text{Mn}_{(\text{DCA})}$, $\text{Fe(II)}_{(\text{oxal})}$, $\text{Fe(III)}_{(\text{oxal})}$, acid volatile sulfur (AVS) and chromium reducible sulfur (CRS) in the sediment at M1 and D3.

Fig. 3. Vertical profiles of O_2 . The slashed area indicates the diffusive boundary layer in the sediment-water interface (SWI). The shaded area indicates that O_2 consumption by aerobic respiration (I and II) and re-oxidation of reduced inorganic compounds (III), respectively.

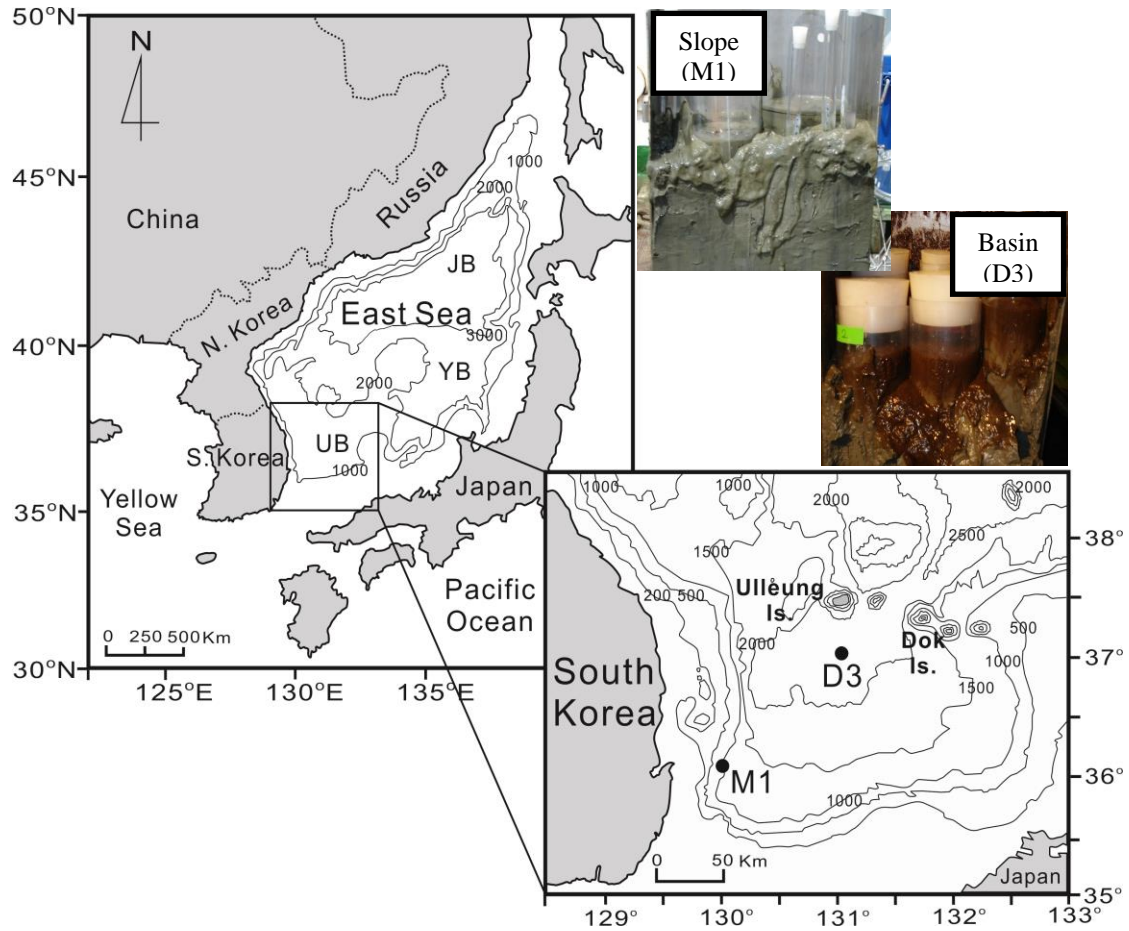
Fig. 4. Changes of concentrations of DIC, Ca^{2+} and Mn^{2+} in pore water and contents of solid phase $\text{Fe(II)}_{(\text{oxal})}$ during anoxic bag incubations of sediments from 0-2, 2-4, 4-6, and 6-8 cm depth at M1 and D3. Data obtained at 8-10 cm depth interval is not shown.

Fig. 5. Vertical distribution of terminal electron acceptors (O_2 , NO_3^- , Mn and Fe) and rates of sulfate reduction measured from whole core analyses, and rates of anaerobic carbon oxidation (DIC production rates), Mn reduction and Fe reduction measured from anoxic bag incubations in Fig. 4. C_{org} by sulfate reduction in panel C and H was calculated from the stoichiometry of 2:1 of C_{org} oxidized to sulfate reduced.

Fig. 6. Depth variations of partitioning of each carbon oxidation pathway in total carbon oxidation at M1 and D3

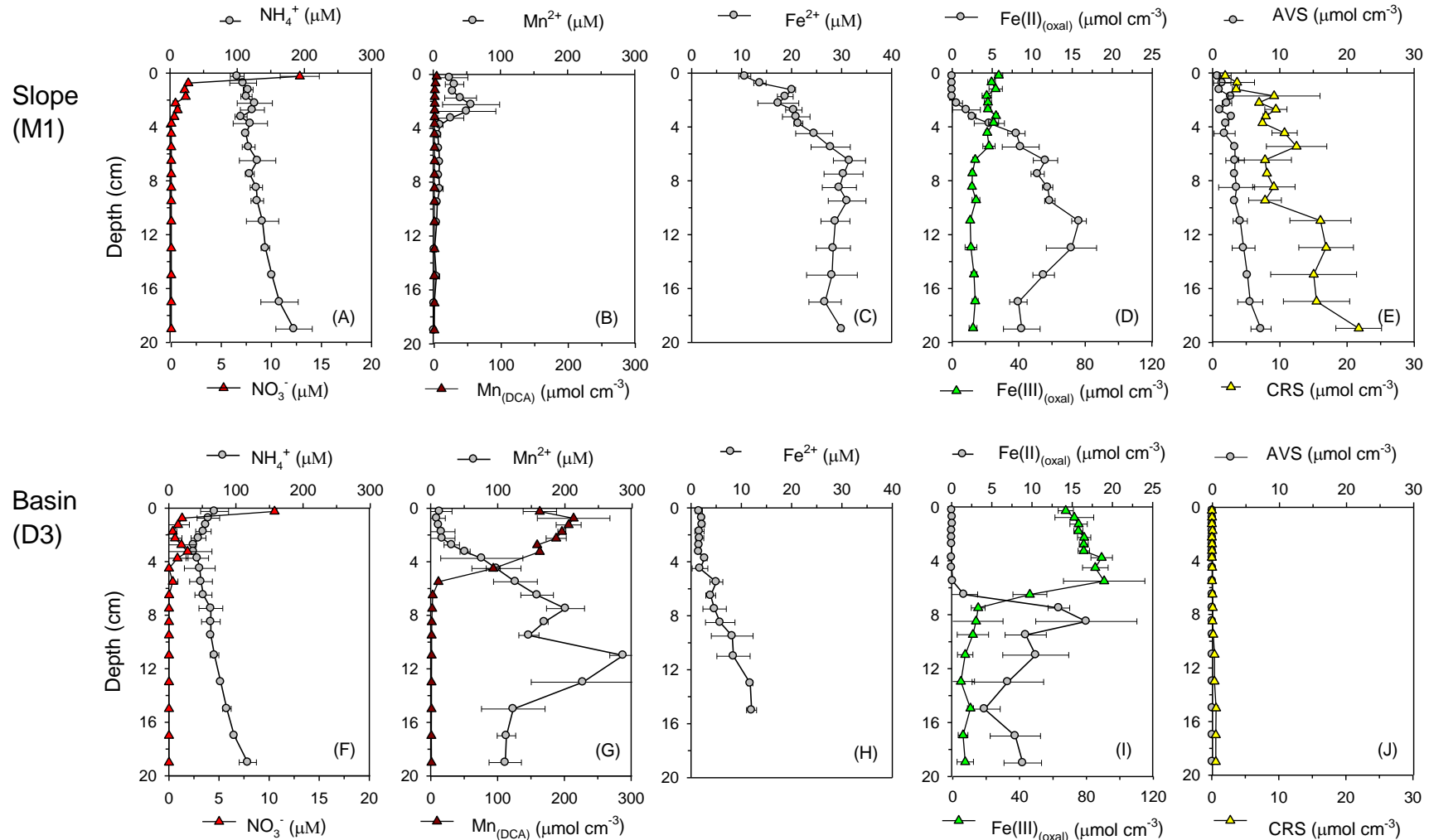
Fig. 7. The relative contribution of Mn reduction to anaerobic carbon oxidation as a function of the content of $\text{Mn}_{(\text{DCA})}$ at 3 different sites. BS, Black Sea (Thamdrup et al., 2000); UB, Ulleung Basin (This study); Sk, Skagerrak (Canfield et al., 1993b).

Hyun et al. – Figure 1 (bg-2016-222)



1 Hyun et al – Figure 2 (bg-2016-222)

2

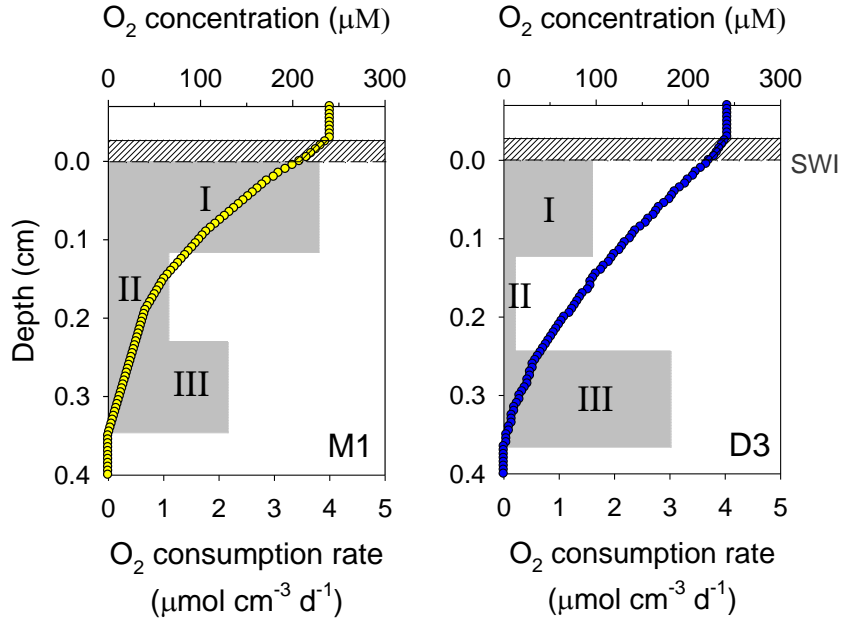


3

4 Hyun et al – Figure 3 (bg-2016-222)

5

6



7

8

9

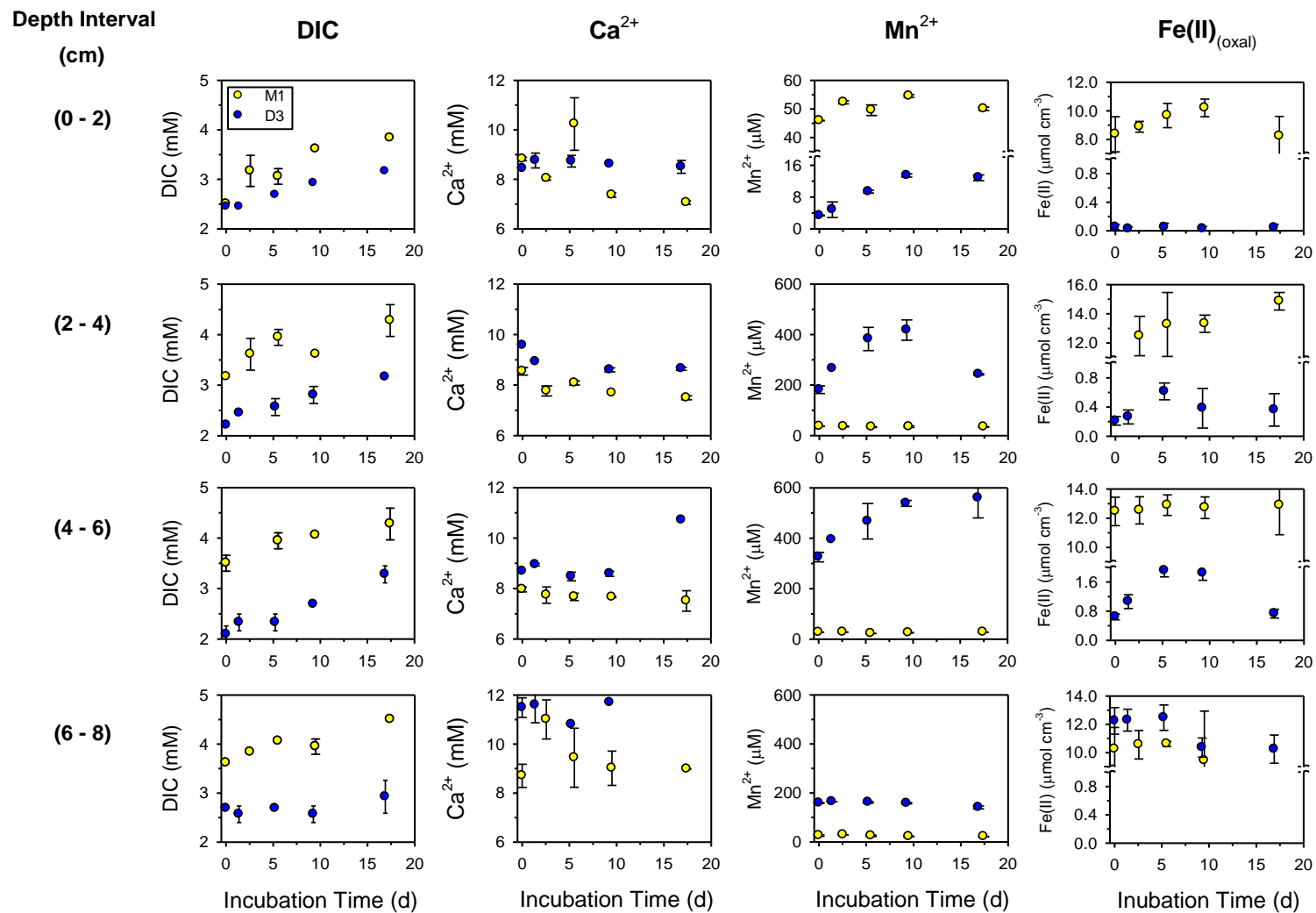
10

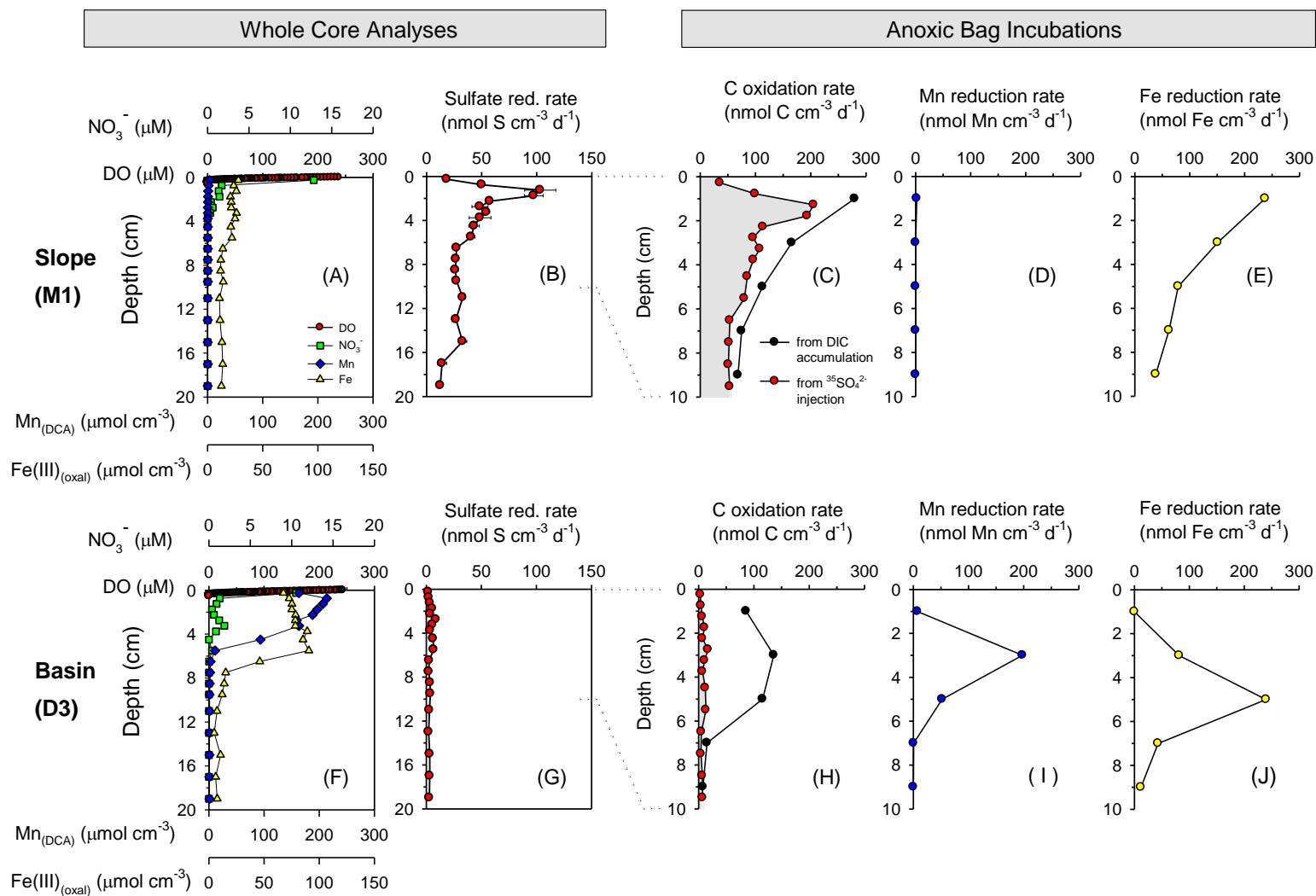
11

12

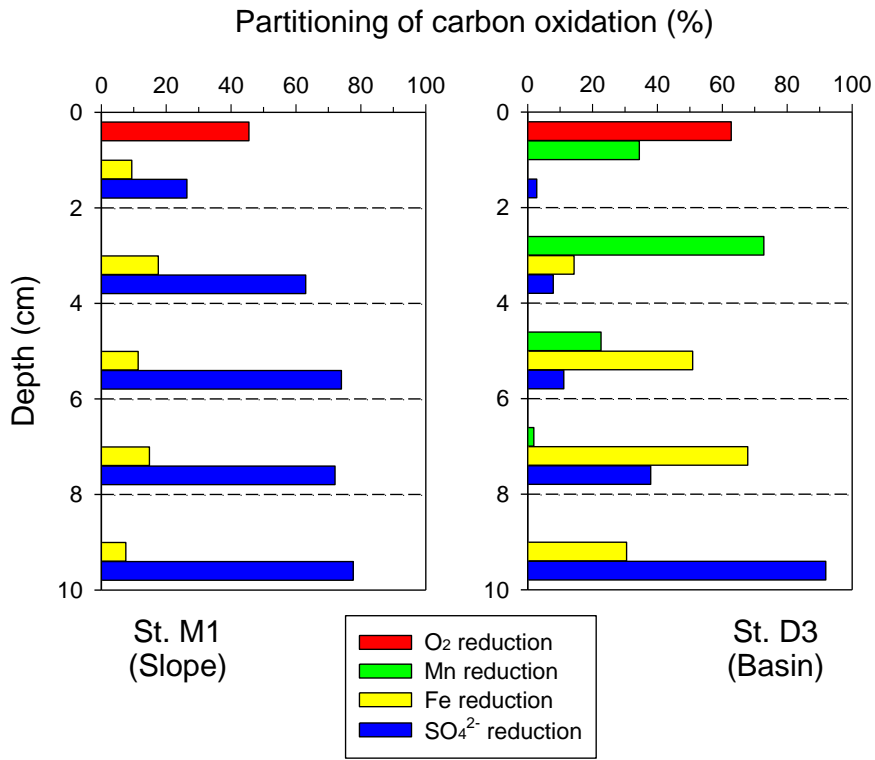
13

14

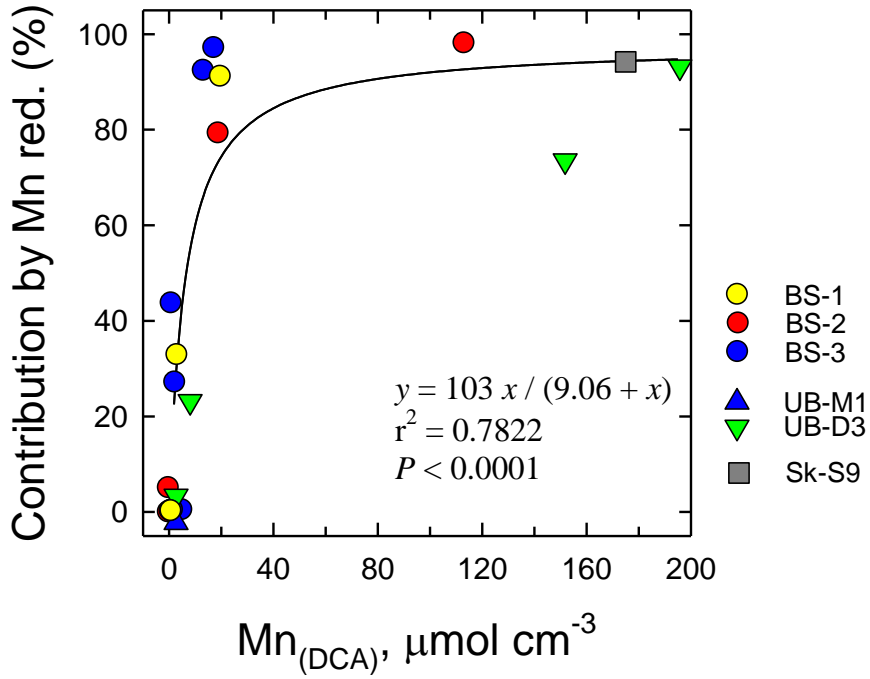




20 Hyun et al. – Figure 6 (bg-2016-222)
21
22



23
24
25
26
27
28



31
32
33
34
35